observed structural features were present in these molecules, including one end with a 58 nm long single stranded region and another end with a sharp kink followed by a region with a beaded appearance lacking appendages. The single stranded region observed is likely to be the poly-U/UC motif which is conserved across HCV genomes [18-24]. The morphology of homopolymeric ssRNA was further verified by imaging an ssRNA transcript of the importin-β coding region prepared *in vitro* with and without a poly(A) tail.

## Materials and Methods

### RNA

The JFH-1 genomic RNA (accession no. AB047639) is a 9678 nt positive strand RNA [60]. The JFH-1 strain, belonging to genotype 2a, is the first strain of the Hepatitis C virus isolated from a patient which could be successfully replicated in cell culture [61]. The JFH-1 RNA used for these experiments was synthesized *in vitro* by T7 polymerase transcription and purified with the Zymoclean kit [62,63]. The polyadenylated importin-β mRNA was prepared *in vitro*. Mouse cDNA for importin-β was cloned into the pTD vector (Shimadzu Corp., Japan) and transcribed with the MEGAscript T7 kit (Ambion, USA). The RNA was polyadenylated with the Poly(A) Tailing kit (Ambion, USA) and purified by LiCl precipitation.

### AFM sample preparation

All pieces of mica were cut with a hole punch and super-glued to a 15 mm metal specimen disc at least a day prior to sample deposition for AFM. The JFH-1 HCV RNA was prepared by diluting the RNA sample to 0.1-0.5 ng/μL in buffer EB (10 mM Tris, pH 8.5) from Qiagen or in a buffer containing 20 mM Tris, 1.5 mM $MgCl_2$, and 1.5 mM dithiothreitol (DTT). The sample was then heated to 65°C for 2 mins, and then kept at room temperature until deposition. Just prior to sample deposition, a piece of mica affixed to a 15 mm metal specimen disc was freshly cleaved and 10 μL 10 mM spermidine was deposited on the mica and incubated for 3.5 mins. The spermidine was then washed away by washing three times with 1 mL of milli-Q water immediately followed by deposition of 10 μL of the RNA sample for 3.5 mins. The sample was then washed again three times with 1 mL of milli-Q water and dried with a stream of nitrogen. The sample was immediately used for AFM imaging.

### AFM imaging and analysis

AFM imaging was performed with the Multimode AFM with a Nanoscope III or IV controller and with an E or a J scanner (Digital instruments, Inc., USA). The microscope was operated in the Tapping Mode™ at a scanning rate of 0.5-1.0 Hz. Rectangular silicon cantilevers with sharpened tetrahedral tips were used (OMCL AC160TS, Olympus Corp., Japan). These probes had a tip radius of about 7 nm, a resonant frequency of about 300 kHz, and a spring constant of about 26 N/m. Images displayed in this publication were flattened in the Nanoscope (v.5.31 r1) software and exported as jpegs. Images were analyzed with the Gwyddion software (Department of Metrology, Czech Metrology Institute, Czech Republic). The raw SPM images were opened in the Gwyddion software and processed by correcting the horizontal scars, correcting lines by matching the height median, leveling the data to make facets point upwards, leveling the data by mean plane subtraction, and removing the polynomial background (3rd degree). The RNA molecules were marked by selecting all molecules above a 0.15-0.20 nm threshold and then removing all grains smaller then 60-70 $px^2$. The edit mask tool in the subtract selection mode was used to deselect molecules from the periphery of the image. The distributions of various grain characteristics were then exported as a raw data file and then the measure individual grain tool was used to click on each molecule and record the zero basis volume and minimum circumcircle radius of each one. The values were inserted into the Origin Lab software (OriginLab Corp., USA), plotted into histograms, and fitted with Gaussian curves to obtain the center value(s) for each histogram. The errors reflect the standard deviation of the Gaussian distribution. The contour length of the molecules was measured and height profiles were generated with the Femtoscan software (Advanced Technologies Center, Moscow, Russia). The scatterplot was plotted and fitted with a linear regression curve with the y-intercept set to 0 in Microsoft Office Excel.

## Results and Discussion

### AFM imaging of HCV RNA tertiary structure

In our experiments, we used the full positive-stranded ssRNA HCV genome which is 9678 nt in length. When the RNA was heated for 2 mins, at 65°C in buffer containing 1.5 mM $MgCl_2$ just prior to deposition on the mica surface for imaging, the RNA molecules had a compact morphology with a variety of appendages extending from the structures (Figure 1A and 1B). A histogram of the volume distribution of these molecules was fitted with a single peak at 3823 ± 1857 $nm^3$ (Figure 1C). The diameter of the smallest enclosing circle for this $Mg^{2+}$-containing buffer was 136 ± 40 nm (Figure 1D). The diameter of HCV viral particles has been reported to be about 30-75 nm [64-74], so the RNA is likely to be compacted 2-5 times more when it is packaged into the capsid.

### AFM imaging of HCV RNA secondary structure

Since $Mg^{2+}$ is required for many tertiary contacts to form, but not required for the formation of RNA secondary structures formed primarily by Watson-Crick base-pairing [57-59], we should be able to image the secondary structure without the formation of tertiary contacts by diluting the RNA in $Mg^{2+}$-free buffer. After heating for 2 mins at 65°C in this buffer just prior to deposition, the morphology of the RNA was markedly different (Figure 2A and 2B). These RNA molecules had a linearized morphology with various small appendages along the molecule. When the volume of these molecules was analyzed, there was a main peak at 4136 ± 1768 $nm^3$ (Figure 2C). This is close to the volume of the HCV genome molecules in the $Mg^{2+}$ buffer (Figure 1C), suggesting that single molecules are observed in both set of conditions. There is also a larger peak in the volume histogram at 8691 ± 436 $nm^3$. This suggests that some of the molecules may actually have dimerized in these images. The diameter of the smallest enclosing circle was 219 ± 63 nm (Figure 2D), 1.6 times larger than the molecules in the $Mg^{2+}$-containing buffer.

### Structural Analysis of HCV RNA

To get a better idea of the secondary structure of the HCV RNA molecules, additional dimensional analysis was performed. In Figure 3, two molecules which appeared to have some structural similarities are shown. These two molecules show a common structural characteristic of one end with a blob with a height of about 2 nm followed by a 35-76 nm long region of the molecule with heights of about 0.5 nm (Figure 3A, left, box outlines). This area likely represents an unpaired single stranded region of the HCV genome. The contour of the molecules extended for lengths of 582 nm (top) and 470 nm (bottom). Height profiles for each of these molecules showed 29 peaks (top) or 27 peaks (bottom) with 17 (top) or 16 (bottom) visibly protruding appendages

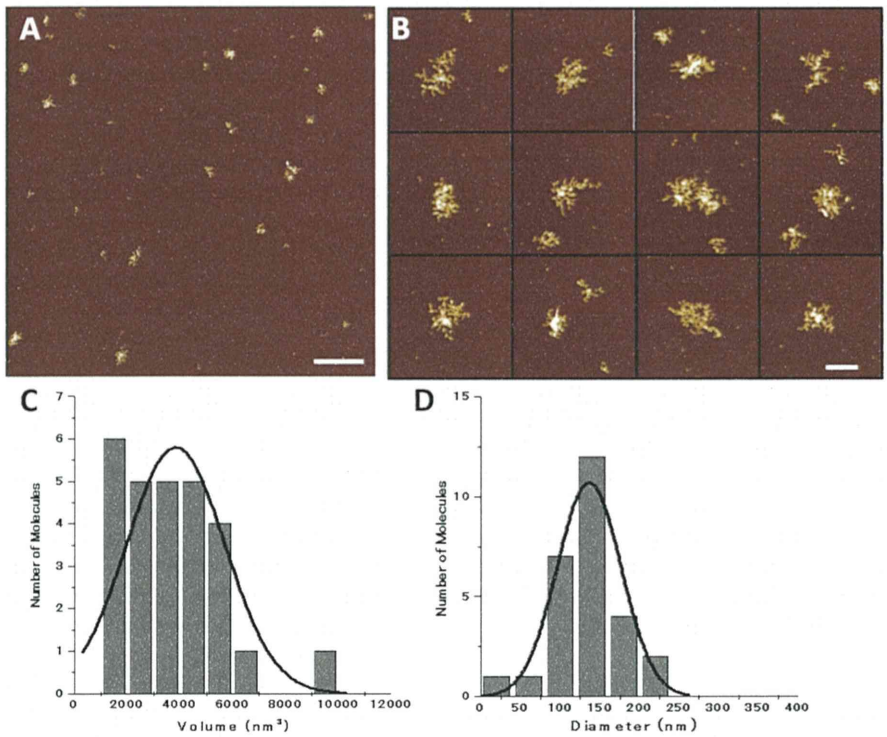


**Figure 1:** AFM imaging and analysis of HCV RNA deposited in $Mg^{2+}$-containing buffer. A representative 3×3 μm² image (**A** scale bar=0.4 μm) along with a gallery of 0.4×0.4 μm² images (**B** scale Bar=0.1 μm) for RNA deposited in buffer containing 1.5 mM $Mg^{2+}$ cations. Histograms of the volume (**C**) and diameter of the smallest enclosing circle (**D**).

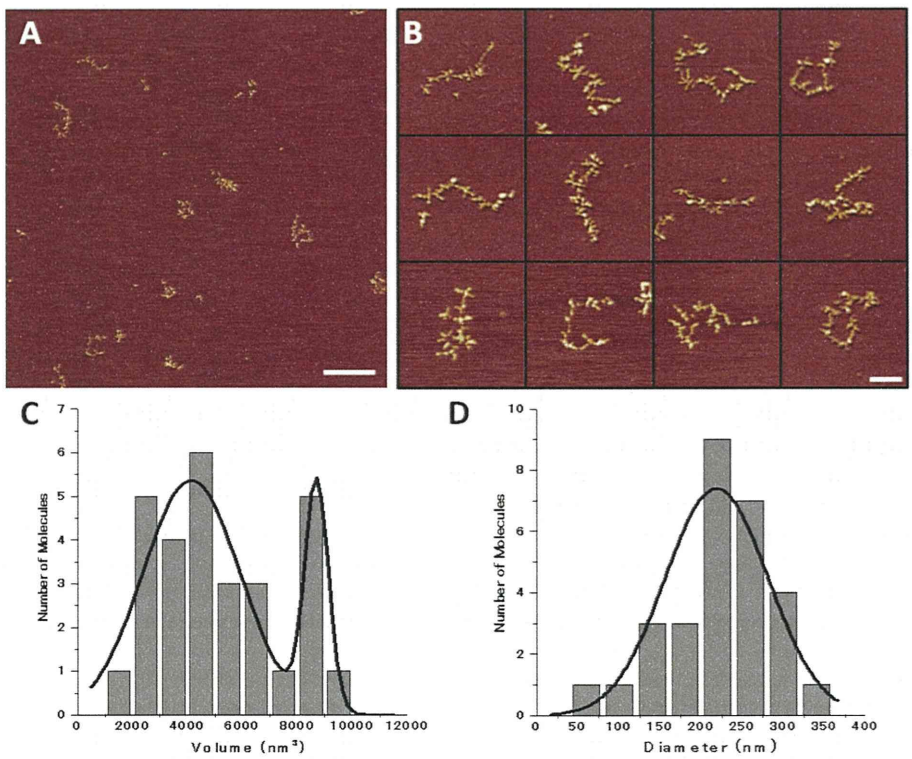


**Figure 2:** AFM imaging and analysis of HCV RNA deposited in $Mg^{2+}$-free buffer. A representative 3×3 μm² image (**A**, scale bar=0.4 μm) along with a gallery of 0.4×0.4 μm² images (**B**, scale Bar=0.1 μm) for RNA deposited in buffer lacking $Mg^{2+}$ cations . Histograms of the volume (**C**) and diameter of the smallest enclosing circle (**D**).

(Figure 3A, graphs). These values can vary considerably depending on the orientation of the molecule on the mica surface. The other end of the molecules has an appendage-free region with a 'beaded' appearance showing variable structures with heights of about 2-3 nm preceded by a sharp kinked region (Figure 3A, left, arrows).

Additional molecules displaying this single-stranded morphology are displayed in Figure 3B. A histogram of the length of this single stranded region results in a single peak centered around the value of 58 ± 8 nm (Figure 3C). It is likely that this region corresponds to the poly-U/UC region present in this RNA molecule. The poly-U/C region is conserved throughout all HCV genotypes, but varies in length [18]. In the JFH-1 genome used in this study, this region is 103 nt long. Varying the length or composition of this region has been reported to effect the efficiency of viral replication [19-21] as well as to influence recognition of the genome by the RIG-I protein which is necessary for the host cell to mount an Interferon (IFN)-mediated immune response to the virus [22-24]. Assuming that this single stranded regions is actually 103 nt long (the whole poly-U/UC region is unpaired and the regions immediately flanking it are paired), it would mean that, according to our measured length (58 nm), the length per nucleotide of the single stranded region is 0.56 nm. In a previous force measurement study with homopolymeric ribonucleotides, molecules 1500-4000 nt in long were stretched to a length of about 1600 nm. This means that the length per nucleotide should be about 0.4-1.0 nm, in good agreement with our calculated value [75,76]. The small blob at the end of the single stranded region is likely the 98 nt 3' X-RNA which is a well studied region immediately flanking the poly-U/UC region and has been reported to form either two or three stem loops [35].

## Verification of RNA homopolymer morphology and ssRNA volume

To further verify the morphology of homopolymeric single-stranded RNA with AFM, an 3890 nt importin-β ssRNA transcript was also imaged (Figure 4). This transcript is not a true mRNA because it lacks the 5' and 3'-UTRs. The importin-β ssRNA was prepared by *in vitro* transcription in two different ways. Initially, the ssRNA was simply transcribed from cDNA with T7 polymerase and directly imaged (Figure 4A). The same RNA was then treated with polyadenylate polymerase to add a random number of adenine residues to the molecules and imaged (Figure 4B). The addition of the poly(A) tail

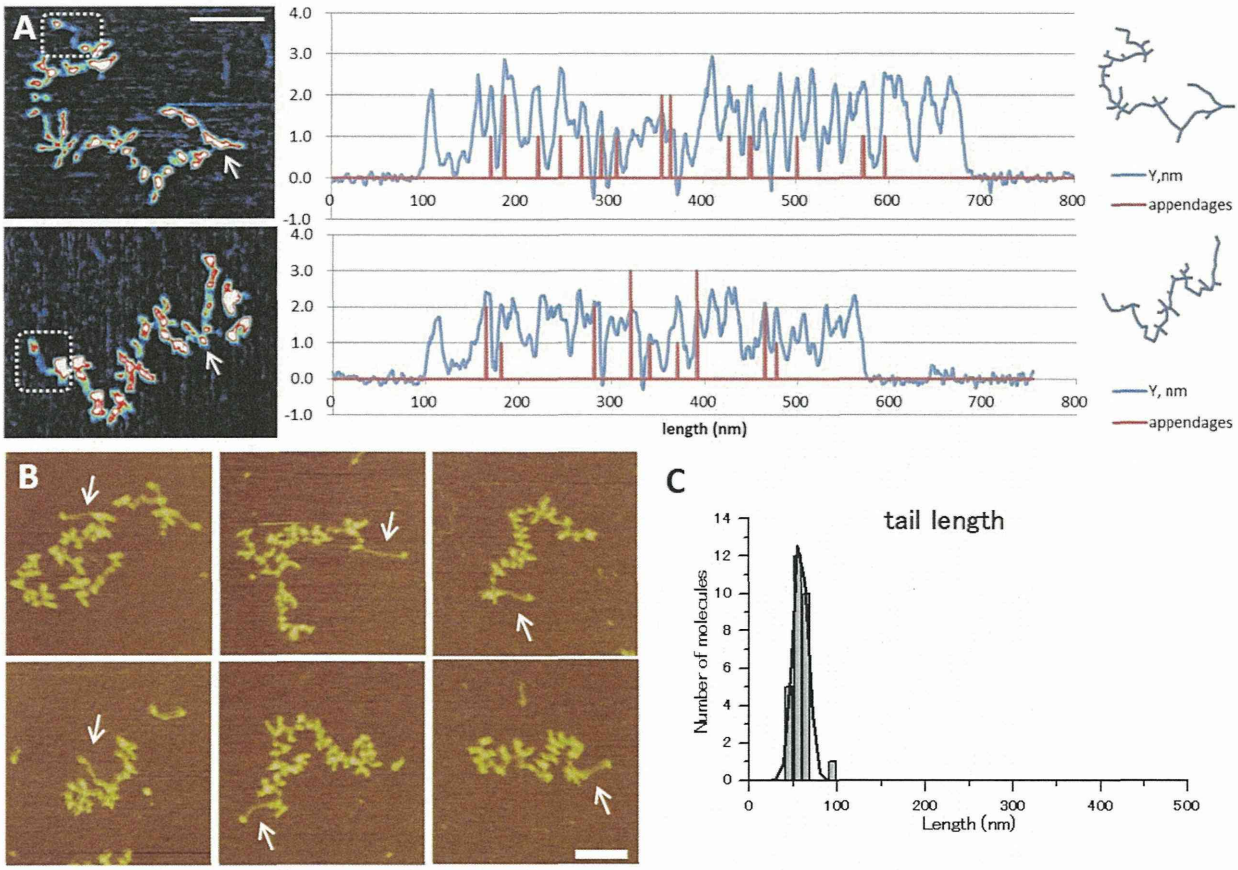


**Figure 3:** Analysis of HCV RNA secondary structure. (**A**) Two representative molecules for $Mg^{2+}$-containing reactions are shown on the left. In these images, black ~0 nm, blue ~0.5 nm, green ~1.0 nm, red ~1.5 nm, and white ~2 nm and higher. The single stranded region of the genome is shown in the dotted box. The arrows point to the kinked region of the genome preceding the appendage-free region of the genome. Bar=80 nm. To the right of each image, a contour plot profile corresponding to each molecule is displayed with the blue line corresponding to the height of features along the length backbone of the molecule and the red line corresponding to the number of appendages protruding out from the molecule along the backbone. Each plot starts at 100 nm along the background of the image. The molecule is then traced starting from the end outlined with the box in the images at the left. A trace of the molecule is shown to the right of each plot. (**B**) Six representative 0.4×0.4 μm² images of molecules exhibiting the single stranded 'tail' morphology → at the end of the molecule. Bar=100 nm (**C**) A histogram of the length of the tail region of the molecules which exhibited this morphology.

shows a single stranded morphology similar to what was observed for the end of the viral RNA molecules. Along the mainly single stranded region, there are often kinks, or 'knobs" and some apparent double-stranded regions. This observation is corroborated by previous AFM imaging which also observed a 'knob' like structures along poly(A) RNA molecules [54]. Additionally, the crystal structure of a poly(A) duplex has been resolved to 1 Å resolution [77].

Measurement of the contour length of the importin-β poly(A) tails showed a very broad distribution of values ranging from 40-830 nm long (Figure 4C). Attempting to fit the broad distribution with a Gaussian curve resulted in a value of 125 ± 88 nm, suggesting that the majority of the poly(A) tails were about twice as long as observed for the viral RNA and the standard deviation of the distribution is 11 times higher. Although the morphologies of the homopolymeric RNA molecules were similar, past studies have reported results suggesting that homopolymeric chains of different nucleotides do not behave exactly the same. For example, poly(G) forms tetrads [78]. Poly(C) and poly(A) have been reported to form single-stranded helical regions which are reflected by plateaus when the chains are stretched resulting from a helix-coil transistion. However, when poly(U) is stretched, there are no plateaus, suggesting that it does not form helical domains [76].

Verification that the viral ssRNA structures we observed represent the full viral genome comes from comparing the measured volumes in of various ssRNA molecules to their molecular weight. The graph in Figure 4D shows how the measured volumes of four different kinds of ssRNA molecules relates to their length in nucleotides. The four molecules analyzed include the HCV RNA (3823 ± 1857 $nm^3$), the importin-β ssRNA without the poly(A) tail (1930 ± 437 $nm^3$), the 28S ribosomal (r)RNA (2688 ± 655 $nm^3$), and the 18S rRNA (921 ± 527 $nm^3$). By fitting these points with a linear regression curve, the volume measured using our method increases by 0.4 $nm^3$ per nucleotide of RNA. Images of the 18S and 28S rRNA molecules are shown in Figure 4E for reference.

## Perspective

The ability of AFM to visualize $Mg^{2+}$-dependent structural changes of RNA opens up an exciting range of possibilities for what AFM can reveal about RNA in the future. For example, the ability of AFM to image molecules in aqueous environments opens up the exciting possibility of visualizing the folding/unfolding transitions of RNA using high-speed AFM (HS-AFM) [41-45]. Additionally, further refinement of the structural models could be gained by imaging individual portions of the

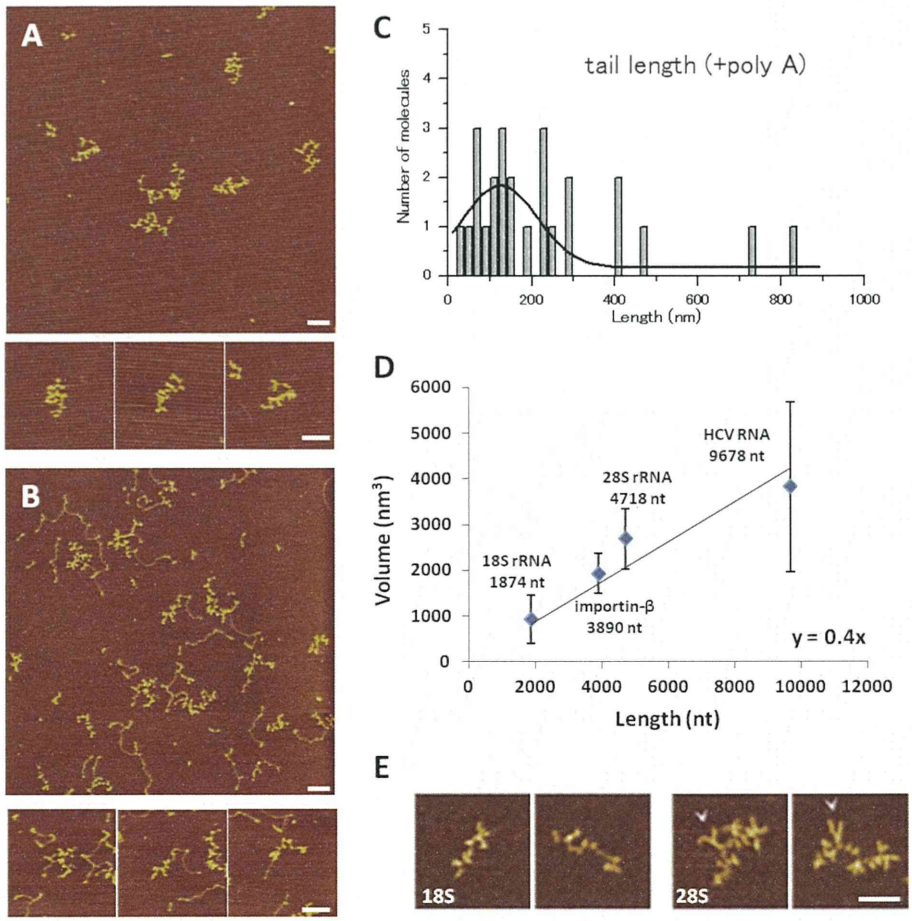


**Figure 4:** Imaging and analysis of importin-β ssRNA secondary structure. Representative 1.5×1.5 μm² images with a gallery of three 0.4×0.4 μm² images of importin-β mRNA without (**A**) and with (**B**) the poly A tail. (**C**) A histogram of the length of the poly(A) tail of the molecules in (**B**). (**D**) A graph demonstrating how the length of four different ssRNA molecules relates to the measured volume. Bars represent the standard deviation of the gaussian distribution. (**E**) Representative images of 18S and 28S rRNA molecules →All scale bars=100 nm.

RNA. Comparing these individual domains may aid in understanding how their structures relate to the structures observed in the full viral genome. Additionally, labeling strategies could be used to identify where a particular sequence may occur along an RNA backbone. In addition to labels, the interaction of various RNA-binding proteins with various RNA structures can also be studied. If a method to attach a RNA-binding protein or chemical to the AFM tip can be developed, recognition imaging [79-82] may also be used to assess which structural features of an RNA molecule the ligand interacts with. Also, proteins can be imaged along with the RNA to observe the effect they have on the viral structure. The ability of AFM to visualize global structural rearrangements of RNA may be a promising tool to investigate the role of RNA structures in viral processes for future studies, which could provide us with an understanding of how to control the spread of the virus in infected individuals.

## Acknowledgements

R.W and K.T. are supported by a Grant-in-Aid for Scientific Research on Innovative Areas "Molecular basis of host cell competency in virus infection" (#24115003) from MEXT Japan. M.K. is supported by a Grant-in-Aid for Scientific Research on Innovative Areas "Spying minority in biological phenomena" (#24115512) from MEXT Japan.

## References

1. World Health Organization (2013) Hepatitis C Fact Sheet no. 164. Geneva, Switzerland.
2. Zhu Y, Chen S (2013) Antiviral treatment of hepatitis C virus infection and factors affecting efficacy. World J Gastroenterol 19: 8963-8973.
3. Choo QL, Kuo G, Weiner a J, Overby LR, Bradley DW, et al. (1989) Isolation of a cDNA clone derived from a blood-borne non-A, non-B viral hepatitis genome. Science 244: 359-362.
4. Tsukiyama-Kohara K1, Iizuka N, Kohara M, Nomoto A (1992) Internal ribosome entry site within hepatitis C virus RNA. J Virol 66: 1476-1483.
5. Brown EA, Zhang H, Ping LH, Lemon SM (1992) Secondary structure of the 5' nontranslated regions of hepatitis C virus and pestivirus genomic RNAs. Nucleic Acids Res 20: 5041-5045.
6. Wang C, Le SY, Ali N, Siddiqui A (1995) An RNA pseudoknot is an essential structural element of the internal ribosome entry site located within the hepatitis C virus 5' noncoding region. RNA 1: 526-537.
7. Honda M, Ping LH, Rijnbrand RC, Amphlett E, Clarke B, et al. (1996) Structural requirements for initiation of translation by internal ribosome entry within genome-length hepatitis C virus RNA. Virology 222: 31-42.
8. Kieft JS, Zhou K, Jubin R, Murray MG, Lau JY, et al. (1999) The hepatitis C virus internal ribosome entry site adopts an ion-dependent tertiary fold. J Mol Biol 292: 513-529.
9. Lukavsky PJ, Otto GA, Lancaster AM, Sarnow P, Puglisi JD (2000) Structures of two RNA domains essential for hepatitis C virus internal ribosome entry site function. Nat Struct Biol 7: 1105-1110.
10. Kieft JS, Zhou K, Grech A, Jubin R, Doudna JA (2002) Crystal structure of an RNA tertiary domain essential to HCV IRES-mediated translation initiation. Nat Struct Biol 9: 370-374.
11. Kim I1, Lukavsky PJ, Puglisi JD (2002) NMR study of 100 kDa HCV IRES RNA using segmental isotope labeling. J Am Chem Soc 124: 9338-9339.
12. Lukavsky PJ1, Kim I, Otto GA, Puglisi JD (2003) Structure of HCV IRES domain II determined by NMR. Nat Struct Biol 10: 1033-1038.
13. Kieft JS (2008) Viral IRES RNA structures and ribosome interactions. Trends Biochem Sci 33: 274-283.
14. Rijnbrand R, Thiviyanathan V, Kaluarachchi K, Lemon SM, Gorenstein DG (2004) Mutational and structural analysis of stem-loop IIIC of the hepatitis C virus and GB virus B internal ribosome entry sites. J Mol Biol 343: 805-817.
15. Lukavsky PJ (2009) Structure and function of HCV IRES domains. Virus Res 139: 166-171.
16. Berry KE, Waghray S, Mortimer SA, Bai Y, Doudna JA (2011) Crystal structure of the HCV IRES central domain reveals strategy for start-codon positioning. Structure 19: 1456-1466.
17. Pérard J, Leyrat C, Baudin F, Drouet E, Jamin M (2013) Structure of the full-length HCV IRES in solution. Nat Commun 4: 1612.
18. Kolykhalov AA, Feinstone SM, Rice CM (1996) Identification of a highly conserved sequence element at the 3 ' terminus of hepatitis C virus genome RNA. These include?: Identification of a Highly Conserved Sequence Element at the 3? Terminus of Hepatitis C Virus Genome RNA. 70: 3363-3371.
19. Friebe P, Bartenschlager R (2002) Genetic analysis of sequences in the 3' nontranslated region of hepatitis C virus that are important for RNA replication. J Virol 76: 5326-5338.
20. Yi M, Lemon SM (2003) 3' nontranslated RNA signals required for replication of hepatitis C virus RNA. J Virol 77: 3557-3568.
21. You S, Rice CM (2008) 3' RNA elements in hepatitis C virus replication: kissing partners and long poly(U). J Virol 82: 184-195.
22. Saito T, Owen DM, Jiang F, Marcotrigiano J, Gale M Jr (2008) Innate immunity induced by composition-dependent RIG-I recognition of hepatitis C virus RNA. Nature 454: 523-527.
23. Uzri D, Gehrke L (2009) Nucleotide sequences and modifications that determine RIG-I/RNA binding and signaling activities. J Virol 83: 4174-4184.
24. Schnell G, Loo YM, Marcotrigiano J, Gale M Jr (2012) Uridine composition of the poly-U/UC tract of HCV RNA defines non-self recognition by RIG-I. PLoS Pathog 8: e1002839.
25. Tuplin A, Wood J, Evans DJ, Patel AH, Simmonds P (2002) Thermodynamic and phylogenetic prediction of RNA secondary structures in the coding region of hepatitis C virus. RNA 8: 824-841.
26. You S, Stump DD, Branch AD, Rice CM (2004) A cis-acting replication element in the sequence encoding the NS5B RNA-dependent RNA polymerase is required for hepatitis C virus RNA replication. J Virol 78: 1352-1366.
27. Lee H, Shin H, Wimmer E, Paul AV (2004) cis-acting RNA signals in the NS5B C-terminal coding sequence of the hepatitis C virus genome. J Virol 78: 10865-10877.
28. Tuplin a, Evans DJ, Simmonds P (2004) Detailed mapping of RNA secondary structures in core and NS5B-encoding region sequences of hepatitis C virus by RNase cleavage and novel bioinformatic prediction methods. J Gen Virol 85: 3037–3047.
29. Zhang J, Yamada O, Sakamoto T, Yoshida H, Araki H, et al. (2005) Inhibition of hepatitis C virus replication by pol III-directed overexpression of RNA decoys corresponding to stem-loop structures in the NS5B coding region. Virology 342: 276-285.
30. Friebe P, Boudet J, Simorre JP, Bartenschlager R (2005) Kissing-loop interaction in the 3' end of the hepatitis C virus genome essential for RNA replication. J Virol 79: 380-392.
31. Diviney S, Tuplin A, Struthers M, Armstrong V, Elliott RM, et al. (2008) A hepatitis C virus cis-acting replication element forms a long-range RNA-RNA interaction with upstream RNA sequences in NS5B. J Virol 82: 9008-9022.
32. Romero-López C, Berzal-Herranz A (2009) A long-range RNA-RNA interaction between the 5' and 3' ends of the HCV genome. RNA 15: 1740-1752.
33. Shetty S, Kim S, Shimakami T, Lemon SM, Mihailescu MR (2010) Hepatitis C virus genomic RNA dimerization is mediated via a kissing complex intermediate. RNA 16: 913-925.
34. Tuplin A, Struthers M, Simmonds P, Evans DJ (2012) A twist in the tail: SHAPE mapping of long-range interactions and structural rearrangements of RNA elements involved in HCV replication. Nucleic Acids Res 40: 6908-6921.
35. Shetty S, Stefanovic S, Mihailescu MR (2013) Hepatitis C virus RNA: molecular switches mediated by long-range RNA-RNA interactions? Nucleic Acids Res 41: 2526-2540.
36. Jaeger JA, SantaLucia J Jr, Tinoco I Jr (1993) Determination of RNA structure and thermodynamics. Annu Rev Biochem 62: 255-287.
37. Hansma PK, Elings VB, Marti O, Bracker CE (1988) Scanning tunneling microscopy and atomic force microscopy: application to biology and technology. Science 242: 209-216.
38. Binnig G, Quate CF, Gerber C (1986) Atomic force microscope. Phys Rev Lett 56: 930-933.
39. Suzuki Y, Yoshikawa Y, Yoshimura SH, Yoshikawa K, Takeyasu K (2011) Unraveling DNA dynamics using atomic force microscopy. Wiley Interdiscip Rev Nanomed Nanobiotechnol.

40. Shlyakhtenko LS, Gilmore J, Portillo A, Tamulaitis G, Siksnys V, et al. (2007) Direct visualization of the EcoRII-DNA triple synaptic complex by atomic force microscopy. Biochemistry 46: 11128-11136.

41. Crampton N, Yokokawa M, Dryden DT, Edwardson JM, Rao DN, et al. (2007) Fast-scan atomic force microscopy reveals that the type III restriction enzyme EcoP15I is capable of DNA translocation and looping. Proc Natl Acad Sci U S A 104: 12755-12760.

42. Gilmore JL, Suzuki Y, Tamulaitis G, Siksnys V, Takeyasu K, et al. (2009) Single-molecule dynamics of the DNA-EcoRII protein complexes revealed with high-speed atomic force microscopy. Biochemistry 48: 10492-10498.

43. Suzuki Y, Higuchi Y, Hizume K, Yokokawa M, Yoshimura SH, et al. (2010) Molecular dynamics of DNA and nucleosomes in solution studied by fast-scanning atomic force microscopy. Ultramicroscopy 110: 682-688.

44. Suzuki Y, Gilmore JL, Yoshimura SH, Henderson RM, Lyubchenko YL, et al. (2011) Visual analysis of concerted cleavage by type IIF restriction enzyme SfiI in subsecond time region. Biophys J 101: 2992-2998.

45. Sanchez H, Suzuki Y, Yokokawa M, Takeyasu K, Wyman C (2011) Protein-DNA interactions in high speed AFM: single molecule diffusion analysis of human RAD54. Integr Biol (Camb) 3: 1127-1134.

46. Suzuki Y, Endo M, Katsuda Y, Ou K, Hidaka K, et al. (2014) DNA origami based visualization system for studying site-specific recombination events. J Am Chem Soc 136: 211-218.

47. Suzuki Y, Endo M, Yang Y, Sugiyama H (2014) Dynamic assembly/disassembly processes of photoresponsive DNA origami nanostructures directly visualized on a lipid membrane surface. J Am Chem Soc 136: 1714-1717.

48. Noestheden M, Hu Q, Tonary AM, Tay LL, Pezacki JP (2007) Evaluation of chemical labeling strategies for monitoring HCV RNA using vibrational microscopy. Org Biomol Chem 5: 2380-2389.

49. Chernov KG, Curmi PA, Hamon L, Mechulam A, Ovchinnikov LP, et al. (2008) Atomic force microscopy reveals binding of mRNA to microtubules mediated by two major mRNP proteins YB-1 and PABP. FEBS Lett 582: 2875-2881.

50. Davis M, Sagan SM, Pezacki JP, Evans DJ, Simmonds P (2008) Bioinformatic and physical characterizations of genome-scale ordered RNA structure in mammalian RNA viruses. J Virol 82: 11824-11836.

51. Sagan SM, Nasheri N, Luebbert C, Pezacki JP (2010) The efficacy of siRNAs against hepatitis C virus is strongly influenced by structure and target site accessibility. Chem Biol 17: 515-527.

52. Wu B1, Grigull J, Ore MO, Morin S, White KA (2013) Global organization of a positive-strand RNA virus genome. PLoS Pathog 9: e1003363.

53. Hansma HG1, Revenko I, Kim K, Laney DE (1996) Atomic force microscopy of long and short double-stranded, single-stranded and triple-stranded nucleic acids. Nucleic Acids Res 24: 713-720.

54. Smith BL, Gallie DR, Le H, Hansma PK (1997) Visualization of poly(A)-binding protein complex formation with poly(A) RNA using atomic force microscopy. J Struct Biol 119: 109-117.

55. Kuznetsov YG, Daijogo S, Zhou J, Semler BL, McPherson A (2005) Atomic force microscopy analysis of icosahedral virus RNA. J Mol Biol 347: 41-52.

56. Archer EJ, Simpson MA, Watts NJ, O'Kane R, Wang B, et al. (2013) Long-range architecture in a viral RNA genome. Biochemistry 52: 3182-3190.

57. Brion P, Westhof E (1997) Hierarchy and dynamics of RNA folding. Annu Rev Biophys Biomol Struct 26: 113-137.

58. Tinoco I Jr, Bustamante C (1999) How RNA folds. J Mol Biol 293: 271-281.

59. Draper DE (2004) A guide to ions and RNA structure. RNA 10: 335-343.

60. Kato T, Furusaka A, Miyamoto M, Date T, Yasui K, et al. (2001) Sequence analysis of hepatitis C virus isolated from a fulminant hepatitis patient. J Med Virol 64: 334-339.

61. Kato T, Date T, Miyamoto M, Furusaka A, Tokushige K, et al. (2003) Efficient replication of the genotype 2a hepatitis C virus subgenomic replicon. Gastroenterology 125: 1808-1817.

62. Kato T, Date T, Murayama A, Morikawa K, Akazawa D, et al. (2006) Cell culture and infection system for hepatitis C virus. Nat Protoc 1: 2334-2339.

63. Wakita T (2009) Isolation of JFH-1 strain and development of an HCV infection system. Methods Mol Biol 510: 305-327.

64. He LF, Alling D, Popkin T, Shapiro M, Alter HJ, et al. (1987) Determining the size of non-A, non-B hepatitis virus by filtration. J Infect Dis 156: 636-640.

65. Yuasa T, Ishikawa G, Manabe S, Sekiguchi S, Takeuchi K, et al. (1991) The particle size of hepatitis C virus estimated by filtration through microporous regenerated cellulose fibre. J Gen Virol 72: 2021-2024.

66. Takahashi K, Kishimoto S, Yoshizawa H, Okamoto H, Yoshikawa A, et al. (1992) p26 protein and 33-nm particle associated with nucleocapsid of hepatitis C virus recovered from the circulation of infected hosts. Virology 191: 431-434.

67. Kaito M, Watanabe S, Tsukiyama-Kohara K, Yamaguchi K, Kobayashi Y, et al. (1994) Hepatitis C virus particle detected by immunoelectron microscopic study. J Gen Virol 75: 1755-1760.

68. Shimizu YK, Feinstone SM, Kohara M, Purcell RH, Yoshikura H (1996) Hepatitis C virus: detection of intracellular virus particles by electron microscopy. Hepatology 23: 205-209.

69. Wakita T, Pietschmann T, Kato T, Date T, Miyamoto M, et al. (2005) Production of infectious hepatitis C virus in tissue culture from a cloned viral genome. Nat Med 11: 791-796.

70. Gastaminza P, Kapadia SB, Chisari FV (2006) Differential biophysical properties of infectious intracellular and secreted hepatitis C virus particles. J Virol 80: 11074-11081.

71. Yu X, Qiao M, Atanasov I, Hu Z, Kato T, et al. (2007) Cryo-electron microscopy and three-dimensional reconstructions of hepatitis C virus particles. Virology 367: 126-134.

72. Nielsen SU, Bassendine MF, Martin C, Lowther D, Purcell PJ, et al. (2008) Characterization of hepatitis C RNA-containing particles from human liver by density and size. J Gen Virol 89: 2507-2517.

73. Gastaminza P, Dryden KA, Boyd B, Wood MR, Law M, et al. (2010) Ultrastructural and biophysical characterization of hepatitis C virus particles produced in cell culture. J Virol 84: 10999-11009.

74. Catanese MT, Uryu K, Kopp M, Edwards TJ, Andrus L, et al. (2013) Ultrastructural analysis of hepatitis C virus particles. Proc Natl Acad Sci U S A 110: 9505-9510.

75. Seol Y, Skinner GM, Visscher K (2004) Elastic properties of a single-stranded charged homopolymeric ribonucleotide. Phys Rev Lett 93: 118102.

76. Seol Y, Skinner GM, Visscher K, Buhot A, Halperin A (2007) Stretching of homopolymeric RNA reveals single-stranded helices and base-stacking. Phys Rev Lett 98: 158103.

77. Safaee N, Noronha AM, Rodionov D, Kozlov G, Wilds CJ, et al. (2013) Structure of the parallel duplex of poly(A) RNA: evaluation of a 50 year-old prediction. Angew Chem Int Ed Engl 52: 10370-10373.

78. Arnott S, Chandrasekaran R, Marttila CM (1974) Structures for polyinosinic acid and polyguanylic acid. Biochem J 141: 537-543.

79. Kienberger F, Ebner A, Gruber HJ, Hinterdorfer P (2006) Molecular recognition imaging and force spectroscopy of single biomolecules. Acc Chem Res 39: 29-36.

80. Dufrêne YF, Hinterdorfer P (2008) Recent progress in AFM molecular recognition studies. Pflugers Arch 456: 237-245.

81. Hirano Y, Takahashi H, Kumeta M, Hizume K, Hirai Y, et al. (2008) Nuclear architecture and chromatin dynamics revealed by atomic force microscopy in combination with biochemistry and cell biology. Pflugers Arch 456: 139-153.

82. Takahashi H, Hizume K, Kumeta M, H Yoshimura S, Takeyasu K (2009) Single-molecule anatomy by atomic force microscopy and recognition imaging. Arch Histol Cytol 72: 217-225.

**Citation:** Gilmore JL, Aizaki H, Yoshida A, Deguchi K, Kumeta M, et al. (2014) Nanoimaging of ssRNA: Genome Architecture of the Hepatitis C Virus Revealed by Atomic Force Microscopy. J Nanomed Nanotechol S5: 010. doi:10.4172/2157-7439.S5-010

This article was originally published in a special issue, Nanotechnology: Challenges & Perspectives in Medicine handled by Editor(s). Dr. Malavosklish Bikram, University of Houston, USA

# Comparison of hepatic arterial infusion chemotherapy and sorafenib in elderly patients with advanced hepatocellular carcinoma: A case series

TOMOYUKI NEMOTO, HIDETAKA MATSUDA, TAKUTO NOSAKA, YASUSHI SAITO, YOSHIHIKO OZAKI, RYOKO HAYAMA, TATSUSHI NAITO, KAZUTO TAKAHASHI, KAZUYA OFUJI, MASAHIRO OHTANI, KATSUSHI HIRAMATSU, HIROYUKI SUTO and YASUNARI NAKAMOTO

Division of Gastroenterology, Second Department of Internal Medicine, Faculty of Medical Sciences, University of Fukui, Fukui 910-1193, Japan

Received May 30, 2014; Accepted July 8, 2014

DOI: 10.3892/mco.2014.371

**Abstract.** Sorafenib and hepatic arterial infusion chemotherapy (HAIC) are both indicated for unresectable hepatocellular carcinoma (HCC). In this study, we compared the efficacy and safety of HAIC to that of sorafenib in elderly patients with HCC. Eligible patients included those aged ≥70 years, with histologically or clinically confirmed advanced HCC. A total of 12 patients received sorafenib (800 mg per day) and 8 patients received HAIC with 5-fluorouracil (300 mg/m$^2$ on days 1-5 and 8-12) with or without cisplatin (20 mg/m$^2$ on days 1 and 8), with interferon-α (3 times per week for 4 weeks). The response rate was significantly higher in patients treated with HAIC (37.5%) compared to that in patients treated with sorafenib (no response). The median overall survival (18.6 and 11.7 months) and progression-free survival (4.0 and 5.0 months) were similar between the sorafenib and HAIC groups, respectively. In the sorafenib group, 58.3% of the patients discontinued treatment compared to none in the HAIC group. The most frequent adverse event leading to discontinuation of sorafenib was anorexia. Similar to sorafenib, HAIC appears to be a feasible treatment and may also have the advantage of an adequate safety profile for elderly patients with advanced HCC. Further study of HAIC in a larger population of elderly patients is required to assess its potential as an alternative to sorafenib for HCC.

*Correspondence to:* Professor Yasunari Nakamoto, Division of Gastroenterology, Second Department of Internal Medicine, Faculty of Medical Sciences, University of Fukui, 23-3 Matsuokashimoaitsuki, Fukui 910-1193, Japan
E-mail: ynakamot@u-fukui.ac.jp

*Key words:* hepatic arterial infusion chemotherapy, interferon, sorafenib, hepatocellular carcinoma, elderly patients, alternative treatment

## Introduction

Hepatocellular carcinoma (HCC) is the most common neoplasm worldwide (1). HCC principally develops on a background of chronic liver disease, particularly cirrhosis caused by hepatitis C or hepatitis B virus infection (1). In Japan, the median age of patients with HCC has been increasing gradually since 1986 (2). Elderly cancer patients often present with multiple comorbidities and age-related changes in the pharmacokinetics and pharmacodynamics of anticancer drugs that may affect chemotherapeutic regimens (3). The clinical benefits of treatment of elderly patients with advanced HCC remain unclear. A previously published study demonstrated that investigations in elderly patients were less intense, that such patients were more likely to receive conservative therapy and that the median survival was worse compared to that among younger patients (4). However, the treatments for HCC have progressed significantly over the last few years and Mirici-Cappa *et al* (5) demonstrated that the overall applicability of radical or effective HCC treatment may not be affected by age. Moreover, Suda *et al* (2) suggested that the therapeutic approach to HCC should not be restricted by patient age.

Sorafenib is an oral tyrosine kinase inhibitor that targets multiple molecular pathways. In a pivotal study, sorafenib provided an overall survival (OS) advantage in patients with advanced HCC, with the median survival increasing by ~3 months in sorafenib-treated patients, compared to those receiving placebo therapy (6). Sorafenib is the only globally approved drug for the treatment of HCC; however, it is not curative and is only indicated for Child-Pugh class A patients who have preserved hepatic function. Hepatic arterial infusion chemotherapy (HAIC) is an alternative option for advanced HCC and, based on the Japanese HCC management guidelines, it is recommended for patients with the same indications for sorafenib (7). Although HAIC is widely used in Japan, as it tends to be associated with a favorable response rate (RR) in patients with HCC, randomized controlled trials have not been conducted and there is currently no evidence of a survival benefit for HAIC. HAIC may reduce HCC stage (8) and is indicated for patients exhibiting a moderate reduction in

hepatic reserve function (9). In patients who achieve a complete response (CR) with HAIC, a long-term survival benefit was reported (10,11). The efficacy of sorafenib treatment in elderly patients with advanced HCC has been investigated in several studies (12-16); however, to the best of our knowledge, there are no available reports regarding the efficacy of HAIC in such patients and there are currently no satisfactory strategies for the management of advanced HCC as a function of age. The aim of this study was to compare the feasibility and safety of HAIC to those of sorafenib in elderly patients with advanced HCC.

## Patients and methods

*Patients.* We retrospectively analyzed data from elderly patients with advanced unresectable HCC, who were treated at our hospital between March, 2002 and June, 2013. Eligible patients included those aged ≥70 years with histologically or clinically confirmed advanced HCC. HCC was considered as unresectable in patients who presented with severe vascular invasion or multiple intrahepatic lesions (i.e., ≥5 nodules), or in those with progressive disease (PD) following surgical or locoregional therapy intervention. A total of 20 eligible patients were identified.

The study protocol was approved by our Institutional Review Board and informed consent was obtained from all the patients prior to treatment.

*Treatment.* In the HAIC group (n=8), an implantable drug delivery system was used for arterial infusion of the chemotherapeutic agents. Between February, 2003 and March, 2009, HAIC consisted of 5-fluorouracil (5-FU) at a dose of 300 mg/m$^2$/day for 5 days during the 1st and 2nd weeks, combined with intramuscular or subcutaneous administration of interferon-α 3 times per week for 4 weeks. Interferon-α dosing consisted of either natural interferon-α, 5 million units; recombinant interferon-α, 12 million units; or interferon-α 2b, 3 million units. From April, 2009 onwards, HAIC was performed with 5-FU plus cisplatin (CDDP) at a dose of 20 mg/m$^2$/day on days 1 and 8, combined with intramuscular interferon-α administration, as described above (17). The treatment cycle was repeated until disease progression or unacceptable drug toxicity.

In the sorafenib group (n=12), a limited number of patients received sorafenib 200-600 mg/day as an initial dose. In the absence of adverse events (AEs), the dose of sorafenib was increased to 400 mg twice daily. Treatment was discontinued on the same basis as in the HAIC group. However, if the performance status and liver function of patients with PD was preserved, sorafenib was continued until the occurrence of severe AEs in order to prevent rapid tumor growth associated with treatment cessation.

*Response assessment.* Tumor response was determined using dynamic computed tomography or magnetic resonance imaging, according to Response Evaluation Criteria in Solid Tumors, version 1.1. RR was defined as the combined percentages of patients experiencing a CR and those with a partial response (PR). Tumor control rate (TCR) was defined as the combined percentages of patients experiencing CR, PR and stable disease (SD). HAIC was evaluated every 6 or 8 weeks and sorafenib treatment was evaluated every 4 or 12 weeks. OS was calculated from the date of treatment initiation to the date of the last follow-up or death. Progression-free survival (PFS) was calculated from the date of treatment initiation to the date

Table I. Clinical characteristics of patients treated with sorafenib and hepatic arterial infusion chemotherapy (HAIC).

| Variables | Sorafenib (n=12) | HAIC (n=8) | P-value |
|---|---|---|---|
| Age (years) | 80.2±5.4 | 74.9±3.4 | 0.039[a] |
| Gender (M/F) | 6/6 | 6/2 | NS[b] |
| White cell count (x10$^2$/μl) | 48.0±13.2 | 59.4±27.4 | NS[a] |
| Lymphocyte count (x10$^2$/μl) | 14.6±8.5 | 14.9±6.2 | NS[a] |
| Platelet count (x10$^4$/μl) | 16.7±6.1 | 14.1±6.7 | NS[a] |
| PT-INR | 1.10±34.6 | 1.16±0.19 | NS[a] |
| ALT (IU/l) | 35.5±0.12 | 41.9±0.19 | NS[a] |
| Total bilirubin (mg/dl) | 0.67±0.40 | 0.76±0.27 | NS[a] |
| Albumin (g/dl) | 3.5±0.4 | 3.3±0.8 | NS[a] |
| Cirrhosis (Child-Pugh A/B/C) | 10/2/0 | 4/4/0 | NS[b] |
| TNM stage (I/II/III/IV-A/IV-B) | 0/2/3/2/5 | 0/2/3/2/1 | NS[c] |
| Largest tumor (mm) | 42.3±21.2 | 49.7±28.2 | NS[a] |
| AFP | 2,027±5,219 | 279±418 | NS[a] |

Results are expressed as means ± standard deviation. [a]Mann-Whitney U test. [b]Fisher's exact test. [c]Chi-square test. M, male; F, female; NS, non-significant; PT-INR, prothrombin time-international normalized ratio; ALT, alanine aminotransferase; Child-Pugh, Child-Pugh classification; TNM, tumor-node-metastasis; AFP, α-fetoprotein.

Table II. Comparison of best response between sorafenib and hepatic arterial infusion chemotherapy (HAIC).

| Response | Sorafenib (n=12) | HAIC (n=8) | P-value |
|---|---|---|---|
| CR | 0 (0.0) | 1 (12.5) | NS |
| PR | 0 (0.0) | 2 (25.0) | NS |
| SD | 6 (50.0) | 4 (50.0) | NS |
| PD | 6 (50.0) | 1 (12.5) | NS |
| RR (CR+PR) | 0 (0.0) | 3 (37.5) | 0.049[a] |
| TCR (CR+PR+SD) | 6 (50.0) | 7 (87.5) | NS |

Values are presented as no. (%). [a]Fisher's exact test. NS, non-significant; CR, complete response; PR, partial response; SD, stable disease; PD, progressive disease; RR, response rate; TCR, tumor control rate.

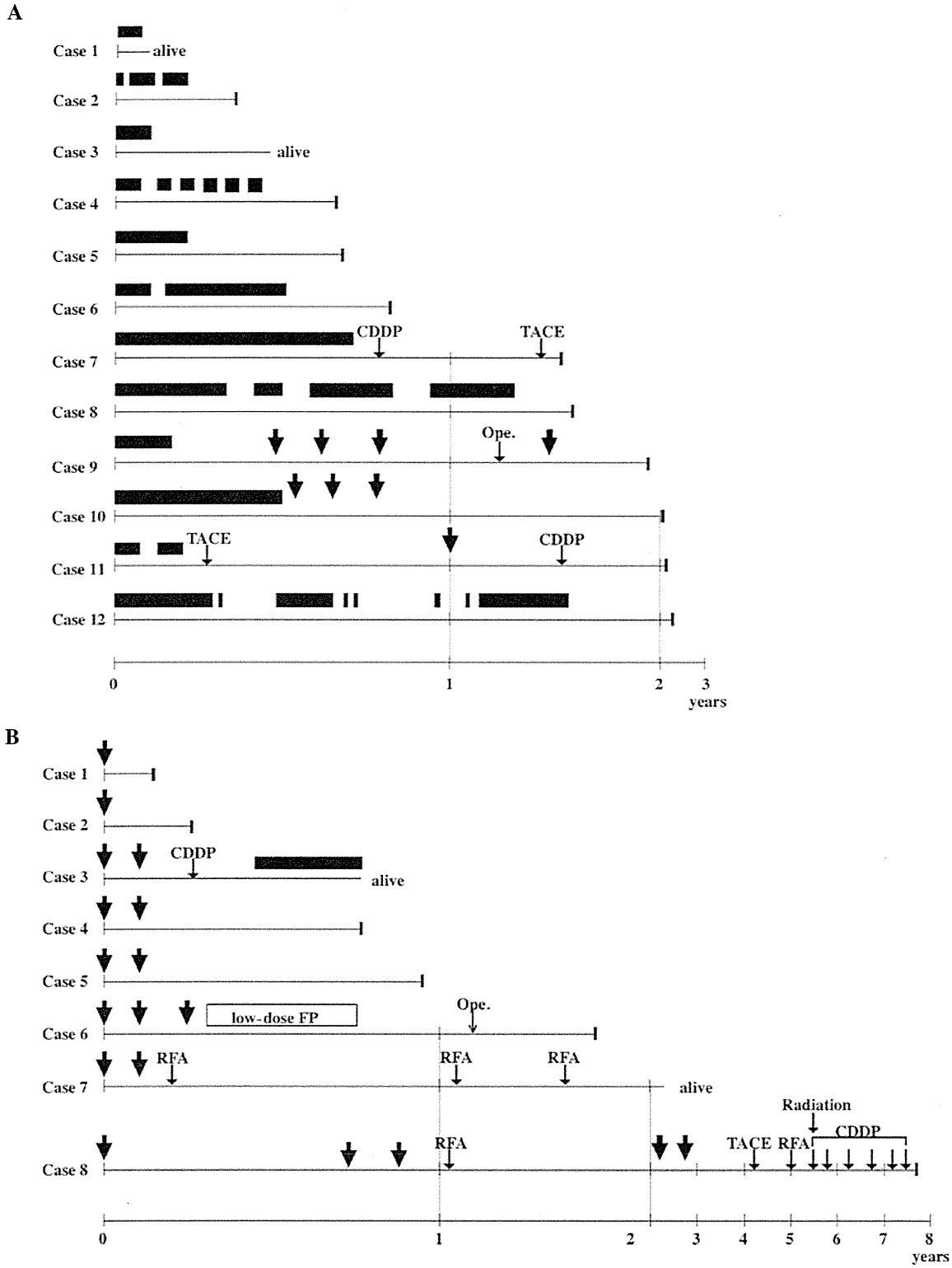


Figure 1. Clinical course of (A) the sorafenib and (B) hepatic arterial infusion chemotherapy (HAIC) groups. The best clinical responses were complete response in 1 patient (case 8) in the HAIC group, partial response in 2 patients (cases 6 and 7) in the HAIC group, stable disease in 10 patients (cases 1, 6, 9, 10, 11 and 12 in the sorafenib group and cases 2, 3, 4 and 5 in the HAIC group) and progressive disease in 7 patients (cases 2, 3, 4, 5, 7 and 8 in the sorafenib group and case 1 in the HAIC group). Although patients 1 and 3 in the sorafenib group and patients 3 and 7 in the HAIC group remained alive, other patients succumbed to the disease at the indicated time points. Closed bars, sorafenib administration. Arrows, HAIC. CDDP, cisplatin infusion; TACE, transcatheter arterial chemoembolization; Ope., operation; low-dose FP, continuous 5-fluorouracil and low-dose cisplatin infusion; RFA, radiofrequency ablation.

of the last follow-up or PD. Drug-related AEs were evaluated according to the Common Toxicity Criteria for Adverse Events, version 4.0 (Japan Clinical Oncology Group/Japan Society of Clinical Oncology edition).

*Additional therapy.* Of the 20 patients, 8 received additional treatment, including surgery, radiofrequency ablation (RFA), transcatheter arterial chemoembolization (TACE), HAIC using 5-FU and low-dose CDDP without interferon-α admin-

istration (low-dose FP), arterial CDDP infusion and irradiation therapy.

*Statistical analyses*. The results are expressed as means ± standard deviation. The differences between the two groups were examined for statistical significance using the Mann-Whitney U test, the Fisher's exact test and the Chi-square test. The survival curves for OS and PFS were analyzed using the Kaplan-Meier method and the differences were evaluated using a log-rank test. The 95% confidence intervals (CIs) of median OS and median PFS were calculated. P<0.05 was considered to indicate a statistically significant difference.

## Results

*Patient characteristics*. The baseline patient clinical characteristics are summarized in Table I. The mean age of the sorafenib group was significantly higher compared to that of the HAIC group (P=0.039). There were no significant differences by blood cell counts, blood coagulation tests, biochemical tests, or Child-Pugh classifiction. In addition, a comparison of tumor-related background factors between the two groups did not reveal any significant differences in TNM stage, main tumor diameter, or serum α-fetoprotein levels.

*Clinical response*. The mean daily dose and duration of sorafenib treatment were 544 mg and 5.3 months, respectively. The mean number of treatment cycles in the HAIC group was 1.8 (~2.2 months). The treatment responses are summarized in Table II. The RR was significantly different between the two groups, as patients in the sorafenib group failed to respond to treatment (P=0.049). However, there was no significant difference in TCR between the two groups. Two patients in the HAIC group achieved a sustained CR after receiving additional RFA: one initially achieved a CR in response to HAIC and the other initially demonstrated a PR in response to HAIC.

*Clinical course and additional therapy*. Fig. 1 shows the clinical course of patients who were treated with sorafenib (Fig. 1A) or HAIC (Fig. 1B). In the sorafenib group, treatment was discontinued in 11 patients; for 7 patients (patients 2, 3, 4, 5, 7, 9 and 11), this was due to drug-related AEs, whereas the remaining patients (patients 6, 8, 10 and 11) developed PD. In the HAIC group, none of the patients discontinued 5-FU and CDDP infusion, but interferon-α administration was discontinued in 1 patient (patient 1). Four patients in each group (patients 7, 9, 10 and 11, Fig. 1A; and patients 3, 6, 7 and 8, Fig. 1B) received various additional therapies, including arterial CDDP infusion (patients 7 and 11, Fig. 1A; and patients 3 and 8, Fig. 1B); operation (patient 9, Fig. 1A; and patient 6, Fig. 1B); TACE (patients 7 and 11, Fig. 1A; and patient 8, Fig. 1B); low-dose FP (patient 6, Fig. 1B); RFA (patients 7 and 8, Fig. 1B); and radiation therapy (patient 8, Fig. 1B). Patients 9 and 10 (Fig. 1A) underwent HAIC immediately after sorafenib failure, whereas patient 3 (Fig. 1B) received sorafenib immediately after HAIC failure. Overall, no patients in the sorafenib group demonstrated a curative response following these treatments, whereas for 3 patients in the HAIC group, the additional treatment was significantly curative (P=0.049).

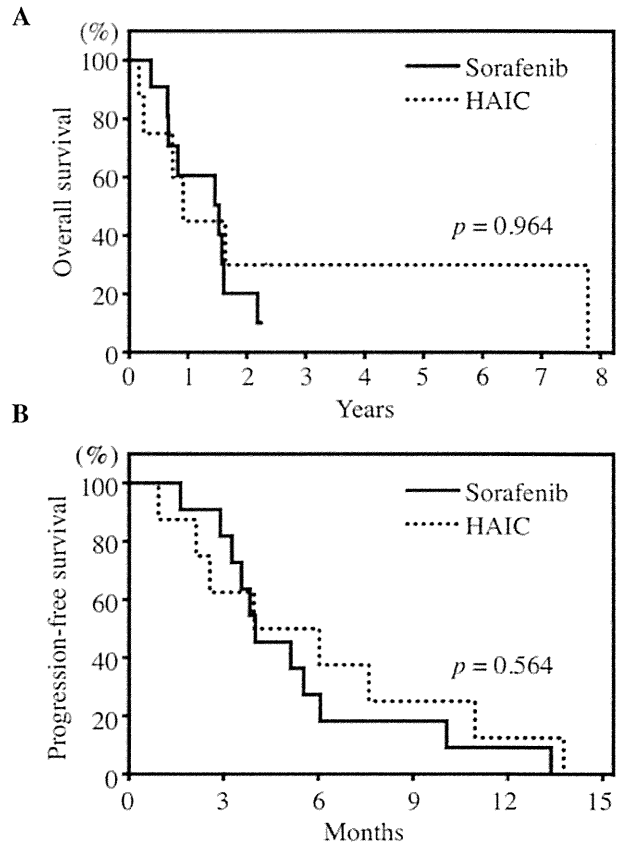


Figure 2. Kaplan-Meier analysis of (A) overall survival and (B) progression-free survival according to sorafenib and hepatic arterial infusion chemotherapy (HAIC). The P-value was calculated using the log-rank test.

*Survival*. The median OS of the total patient population was 17.8 months (0.93-94.7 months). The median OS was 18.6 months (95% CI: 13.8-23.4) and 11.7 months (95% CI: 0-31.5) in the sorafenib and HAIC groups, respectively (Fig. 2A). The median PFS was 4.0 months (95% CI: 2.1-5.9) and 5.0 months (95% CI: 2.6-7.4) in the sorafenib and HAIC groups, respectively (Fig. 2B). The median OS and PFS were not significantly different between the two groups (P=0.964 and 0.562, respectively).

*Safety*. The major AEs are listed in Table III. A total of 7 patients (58.3%) in the sorafenib group discontinued treatment due to grade 3 AEs [4 patients, anorexia; and 1 patient each with hand-foot (HF) syndrome, ascites and hepatic encephalopathy], whereas no patients demonstrated intolerance to HAIC. The discontinuation rate in the sorafenib group was significantly higher compared to that in the HAIC group (P=0.015). Among sorafenib-treated patients, the most frequent AEs were mild in severity (grade 1/2) and included HF syndrome, anorexia, hypoalbuminemia and diarrhea. Grade 3 AEs included HF syndrome, anorexia and hypertension. One Child-Pugh class A patient developed hepatic failure (hepatic encephalopathy) and sorafenib was discontinued. There were no grade 4 AEs. Among HAIC group patients, the most frequent AEs were mostly mild in severity (grade 1/2) and included decreased platelet count, anemia, fever, malaise, anorexia, hypoalbuminemia, decreased white blood cell count and decreased neutrophil count. In total, 6 hematological

Table III. Adverse events.

| | Sorafenib (n=12) Grade (CTCAE v4.0) | | | | | | HAIC (n=8) Grade (CTCAE v4.0) | | | | | |
|---|---|---|---|---|---|---|---|---|---|---|---|---|
| Adverse events | 1 | 2 | 3 | 4 | Any | 3-4 | 1 | 2 | 3 | 4 | Any | 3-4 |
| Anemia | 4 | 1 | | | 5 (41.7) | 0 | 2 | 5 | | | 7 (87.5) | 0 |
| Decreased WBC | | 1 | | | 1 (8.3)[a] | 0 | 2 | 3 | 1 | | 6 (75.0)[a] | 1 (12.5) |
| Decreased neutrophil count | | 1 | | | 1 (8.3)[a] | 0 | 3 | 2 | 1 | | 6 (75.0)[a] | 1 (12.5) |
| Decreasedlatelet count | 4 | 3 | 1 | | 8 (66.7) | 1 (8.3) | 3 | | 3 | 1 | 7 (87.5) | 4 (50.0) |
| Malaise | 5 | 2 | | | 7 (58.3) | 0 | 4 | 3 | | | 7 (87.5) | 0 |
| Fever | | | | | 0[b] | 0 | 6 | 1 | | | 7 (87.5)[b] | 0 |
| Anorexia | 2 | 4 | 3 | | 9 (75.0) | 3 (25.0) | 3 | 4 | | | 7 (87.5) | 0 |
| Nausea | 1 | | | | 1 (8.3) | 0 | 2 | | | | 2 (25.0) | 0 |
| Vomiting | | | | | 0 | 0 | | | | | 0 | 0 |
| Diarrhea | 2 | 7 | | | 9 (75.0) | 0 | 2 | | | | 2 (25.0) | 0 |
| Mucositis | 1 | 2 | | | 3 (25.0) | 0 | | 1 | | | 1 (12.5) | 0 |
| Hand-foot syndrome | 4 | 1 | 4 | | 9 (75.0)[a] | 4 (33.3) | | | | | 0[a] | 0 |
| Hepatic encephalopathy | | | 1 | | 1 (8.3) | 1 (8.3) | | | | | 0 | 0 |
| Ascites | | 3 | | | 3 (25.0) | 0 | | | | | 0 | 0 |
| Bleeding | | | | | 0 | 0 | | | | | 0 | 0 |
| Cardiological | | | | | 0 | 0 | | | | | 0 | 0 |
| Hypertension | 2 | 3 | 3 | | 8 (66.7)[a] | 3 (25.0) | | | | | 0[a] | 0 |
| Pancreatitis | | | | | 0 | 0 | | | | | 0 | 0 |
| Infection | | 1 | | | 1 (8.3) | 0 | | 2 | | | 2 (25.0) | 0 |
| Hyperbilirubinemia | 2 | 1 | | | 3 (25.0) | 0 | 2 | | | | 2 (25.0) | 0 |
| Hypoalbuminemia | 2 | 8 | | | 10 (83.3) | 0 | 1 | 5 | | | 6 (75.0) | 0 |
| Increased AST | 6 | | | | 6 (50.0) | 0 | 2 | | | | 2 (25.0) | 0 |
| Increased ALT | 3 | | | | 3 (25.0) | 0 | 1 | | | | 1 (12.5) | 0 |
| Increased creatinine | 1 | | | | 1 (8.3) | 0 | 1 | 2 | | | 3 (37.5) | 0 |
| Increased serum amylase | 3 | 2 | | | 5 (41.7) | 0 | | | | | 0 | 0 |

The values represent number of events and the parenthetical data represent percentage values. [a]P<0.01; [b]P<0.001 (Fisher's exact test). CTCAE v4.0, Common Terminology Criteria for Adverse Events, version 4.0; WBC, white blood cell; AST, aspartate aminotransferase; ALT, alanine aminotransferase.

AEs of grade 3/4 were recorded in 4 patients. In the HAIC group, 1 patient (12.5%) experienced catheter occlusion as a catheter-related complication. In addition, 5 patients in the sorafenib group changed Child-Pugh class from A to B, whereas none of the patients in the HAIC group changed Child-Pugh class. These changes were mostly caused by the development of hypoalbuminemia in sorafenib-treated patients; there was no significant change in the prothrombin time-international normalized ratio (PT-INR).

## Discussion

In the present study, we demonstrated the feasibility and safety of HAIC in elderly patients with advanced HCC. Several previous studies demonstrated the efficacy and safety of sorafenib in elderly patients (12,14-16); however, to the best of our knowledge, there are no studies performing a comparison of efficacy and safety between sorafenib and HAIC in elderly patients with HCC. It should be noted that the definition of 'elderly' may be controversial. We selected the cut-off age of 70 years, as the majority of age-related changes occur after this age (3). There are some studies available comparing sorafenib and HAIC for the treatment of HCC, but they were not performed in elderly patients (18,19).

In the present study, the RR of the HAIC group was significantly higher compared to that of the sorafenib group, but the TCR was similar between the two groups. Our findings were concurrent with those of previous studies of interferon-α-containing HAIC that demonstrated a RR of 24.6-73.0% (11,17,20-24), indicating that interferon-α-containing HAIC is a feasible treatment for elderly patients with advanced HCC.

An important finding of the present study is that, in the HAIC group, over a third of the patients achieved a CR or PR and, among these patients, 3 achieved long-term survival with additional curative therapy. This observation has important implications in understanding the indications for HAIC in elderly patients. There were no significant differences in median OS and PFS between the two groups. The median PFS with sorafenib was similar to that reported by previous

investigations in elderly patients, but the median OS was longer (12,14-16). The reasons underlying the prolongation of OS in the sorafenib group in the present study are unknown, but one possibility is that the sorafenib group included 2 patients who received HAIC immediately after disease progression, which may skew the data. Two patients in the HAIC group achieved a CR after additional RFA. Other studies have demonstrated that a CR may improve long-term survival, although this was demonstrated in elderly patients (10,11).

The rate of treatment discontinuation due to severe AEs was significantly higher in the sorafenib group compared to that in the HAIC group. Multiple AEs have been associated with 5-FU, CDDP and interferon-α therapy; however, life-threatening AEs rarely occur, even in patients with liver cirrhosis (11,17,20,23). In this study, AEs in HAIC-treated patients were more severe than previously reported (11,17,20,23), particularly thrombocytopenia, although none resulted in treatment discontinuation or required any additional management. The evaluation of AEs in this patient population may be challenging, as the majority of the patients already presented with pancytopenia due to underlying liver cirrhosis. However, a high AE-induced discontinuation rate was apparent among sorafenib-treated patients, mostly as a result of anorexia or hypoalbuminemia, which may lead to ascites. In the present study, patients with a mean age of 80.2 years comprised 75% of all the grades of anorexia. This is concordant with the observations of Morimoto *et al* (13), who indicated that the incidence of anorexia was significantly higher among patients aged ≥75 years. Our results and those of Morimoto *et al* (13) differ from the results of the SHARP and Asia-Pacific trials (6,25); however, in those studies, the age and incidence of all-grade anorexia was 64.9 years (mean) and 51 years (median) and 14 and 12.8%, respectively (6,25). The results of those studies and our present results suggest that elderly patients are more prone to sorafenib-induced anorexia. In addition, Montella *et al* (15) suggested that the changes reported in Child-Pugh scores, as a result of changes in hypoalbuminemia and PT-INR, appeared to be associated with liver function and worsening of cirrhosis, rather than to the drugs administered. However, in the elderly patients in this study, the PT-INR did not change, suggesting preserved hepatic protein synthesis, indicating that hypoalbuminemia may be associated with the anorexia, rather than liver dysfunction. Accordingly, the results of the present study suggest that hypoalbuminemia is an important AE in elderly patients. In summary, HAIC may be a safer option compared to sorafenib for the treatment of elderly patients with HCC.

There were several limitations in the interpretation of the data presented in this study. First, the retrospective design and limited number of patients enrolled may give rise to selection bias. The mean age of the sorafenib group was higher compared to that of the HAIC group, which may explain why the incidence of AEs was higher in the sorafenib group. Moreover, according to the initial response to treatment, additional therapies were performed without limitation, which may affect OS. All the patients in the sorafenib group who received additional therapies developed PD or severe AEs, while some of the patients in the HAIC group who received additional therapies achieved a CR or PR. However, in part, the present study provided significant information regarding the management of HCC in elderly patients.

In conclusion, HAIC appears to be a feasible and safe treatment option for elderly patients with advanced HCC. However, further study of HAIC in a larger population of elderly patients is required to assess its potential as an alternative option for HCC management.

## Acknowledgements

This study was supported, in part, by a grant from the Clinical Trial and Advanced Medical Center of University of Fukui.

## References

1. El-Serag HB: Epidemiology of viral hepatitis and hepatocellular carcinoma. Gastroenterology 142: 1264-1273, 2012.
2. Suda T, Nagashima A, Takahashi S, *et al*: Active treatments are a rational approach for hepatocellular carcinoma in elderly patients. World J Gastroenterol 19: 3831-3840, 2013.
3. Balducci L: Geriatric oncology: challenges for the new century. Eur J Cancer 36: 1741-1754, 2000.
4. Collier JD, Curless R, Bassendine MF and James OF: Clinical features and prognosis of hepatocellular carcinoma in Britain in relation to age. Age Ageing 23: 22-27, 1994.
5. Mirici-Cappa F, Gramenzi A, Santi V, *et al*: Treatments for hepatocellular carcinoma in elderly patients are as effective as in younger patients: a 20-year multicentre experience. Gut 59: 387-396, 2010.
6. Llovet JM, Ricci S, Mazzaferro V, *et al*: Sorafenib in advanced hepatocellular carcinoma. N Engl J Med 359: 378-390, 2008.
7. Kudo M, Izumi N, Kokudo N, *et al*; HCC Expert Panel of Japan Society of Hepatology: Management of hepatocellular carcinoma in Japan: Consensus-Based Clinical Practice Guidelines proposed by the Japan Society of Hepatology (JSH) 2010 updated version. Dig Dis 29: 339-364, 2011.
8. Meric F, Patt YZ, Curley SA, *et al*: Surgery after downstaging of unresectable hepatic tumors with intra-arterial chemotherapy. Ann Surg Oncol 7: 490-495, 2000.
9. Miyaki D, Aikata H, Honda Y, *et al*: Hepatic arterial infusion chemotherapy for advanced hepatocellular carcinoma according to Child-Pugh classification. J Gastroenterol Hepatol 27: 1850-1857, 2012.
10. Ando E, Tanaka M, Yamashita F, *et al*: Hepatic arterial infusion chemotherapy for advanced hepatocellular carcinoma with portal vein tumor thrombosis: analysis of 48 cases. Cancer 95: 588-595, 2002.
11. Obi S, Yoshida H, Toune R, *et al*: Combination therapy of intraarterial 5-fluorouracil and systemic interferon-alpha for advanced hepatocellular carcinoma with portal venous invasion. Cancer 106: 1990-1997, 2006.
12. Wong H, Tang YF, Yao TJ, *et al*: The outcomes and safety of single-agent sorafenib in the treatment of elderly patients with advanced hepatocellular carcinoma (HCC). Oncologist 16: 1721-1728, 2011.
13. Morimoto M, Numata K, Kondo M, *et al*: Higher discontinuation and lower survival rates are likely in elderly Japanese patients with advanced hepatocellular carcinoma receiving sorafenib. Hepatol Res 41: 296-302, 2011.
14. Di Costanzo GG, Tortora R, De Luca M, *et al*: Impact of age on toxicity and efficacy of sorafenib-targeted therapy in cirrhotic patients with hepatocellular carcinoma. Med Oncol 30: 446, 2013.
15. Montella L, Addeo R, Cennamo G, *et al*: Sorafenib in elderly patients with advanced hepatocellular carcinoma: a case series. Oncology 84: 265-272, 2013.
16. Jo M, Yasui K, Kirishima T, *et al*: Efficacy and safety of sorafenib in very elderly patients aged 80 years and older with advanced hepatocellular carcinoma. Hepatol Res: Feb 14, 2014 (Epub ahead of print).
17. Yamashita T, Arai K, Sunagozaka H, *et al*: Randomized, phase II study comparing interferon combined with hepatic arterial infusion of fluorouracil plus cisplatin and fluorouracil alone in patients with advanced hepatocellular carcinoma. Oncology 81: 281-290, 2011.
18. Hiramine Y, Uto H, Imamura Y, *et al*: Sorafenib and hepatic arterial infusion chemotherapy for unresectable advanced hepatocellular carcinoma: A comparative study. Exp Ther Med 2: 433-441, 2011.

19. Jeong SW, Jang JY, Lee JE, *et al*: The efficacy of hepatic arterial infusion chemotherapy as an alternative to sorafenib in advanced hepatocellular carcinoma. Asia Pac J Clin Oncol 8: 164-171, 2012.
20. Kasai K, Ushio A, Kasai Y, *et al*: Therapeutic efficacy of combination therapy with intra-arterial 5-fluorouracil and systemic pegylated interferon alpha-2b for advanced hepatocellular carcinoma with portal venous invasion. Cancer 118: 3302-3310, 2012.
21. Enjoji M, Morizono S, Kotoh K, *et al*: Re-evaluation of antitumor effects of combination chemotherapy with interferon-alpha and 5-fluorouracil for advanced hepatocellular carcinoma. World J Gastroenterol 11: 5685-5687, 2005.
22. Ota H, Nagano H, Sakon M, *et al*: Treatment of hepatocellular carcinoma with major portal vein thrombosis by combined therapy with subcutaneous interferon-alpha and intra-arterial 5-fluorouracil; role of type 1 interferon receptor expression. Br J Cancer 93: 557-564, 2005.
23. Nagano H, Wada H, Kobayashi S, *et al*: Long-term outcome of combined interferon-alpha and 5-fluorouracil treatment for advanced hepatocellular carcinoma with major portal vein thrombosis. Oncology 80: 63-69, 2011.
24. Uka K, Aikata H, Takaki S, *et al*: Pretreatment predictor of response, time to progression, and survival to intraarterial 5-fluorouracil/interferon combination therapy in patients with advanced hepatocellular carcinoma. J Gastroenterol 42: 845-853, 2007.
25. Cheng AL, Kang YK, Chen Z, *et al*: Efficacy and safety of sorafenib in patients in the Asia-Pacific region with advanced hepatocellular carcinoma: a phase III randomised, double-blind, placebo-controlled trial. Lancet Oncol 10: 25-34, 2009.

# A peptide antigen derived from EGFR T790M is immunogenic in non-small cell lung cancer

KAZUYA OFUJI[1,2], YOSHITAKA TADA[1,3], TOSHIAKI YOSHIKAWA[1], MANAMI SHIMOMURA[1], MAYUKO YOSHIMURA[1], KEIGO SAITO[1], YASUNARI NAKAMOTO[2] and TETSUYA NAKATSURA[1]

[1]Division of Cancer Immunotherapy, Exploratory Oncology Research and Clinical Trial Center, National Cancer Center, Kashiwa, Chiba; [2]Second Department of Internal Medicine, Faculty of Medical Sciences, University of Fukui, Fukui; [3]Research Institute for Biomedical Sciences, Tokyo University of Science, Noda, Chiba, Japan

Received August 29, 2014; Accepted October 9, 2014

DOI: 10.3892/ijo.2014.2787

**Abstract.** Lung cancer is the leading cause of cancer-related deaths worldwide. Epidermal growth factor receptor-tyrosine kinase inhibitors (EGFR-TKIs), such as gefitinib and erlotinib, have demonstrated marked clinical activity against non-small cell lung cancer (NSCLC) harboring activating epidermal growth factor receptor (EGFR) mutations. However, in most cases, patients develop acquired resistance to EGFR-TKI therapy. The threonine to methionine change at codon 790 of EGFR (EGFR T790M) mutation is the most common acquired resistance mutation, and is present in ~50% cases of TKI resistance. New treatment strategies for NSCLC patients harboring the EGFR T790M mutation are required. We evaluated the immunogenicity of an antigen derived from EGFR with the T790M mutation. Using BIMAS we selected several EGFR T790M-derived peptides bound to human leukocyte antigen (HLA)-A*02:01. T790M-A peptide (789-797) (IMQLMPFGC)-specific cytotoxic T lymphocytes (CTLs) were induced from peripheral blood mononuclear cells (PBMCs) of HLA-A2$^+$ healthy donors. An established T790M-A-specific CTL line showed reactivity against the NCSLC cell line, H1975-A2 (HLA-A2$^+$, T790M$^+$), but not H1975 (HLA-A2$^-$, T790M$^+$), and the corresponding wild-type peptide (ITQLMPFGC)-pulsed T2 cells using an interferon-γ (IFN-γ) enzyme-linked immuno spot (ELISPOT) assay. This CTL line also demonstrated peptide-specific cytotoxicity against H1975-A2 cells. This finding suggests that the EGFR T790M mutation-derived antigen could be a new target for cancer immunotherapy.

*Correspondence to:* Professor Tetsuya Nakatsura, Division of Cancer Immunotherapy, Exploratory Oncology Research and Clinical Trial Center, National Cancer Center, 6-5-1 Kashiwanoha, Kashiwa, Chiba 277-8577, Japan
E-mail: tnakatsu@east.ncc.go.jp

*Abbreviations:* aAPC, artificial antigen-presenting cell; ELISPOT, enzyme-linked immuno spot; HLA, human leukocyte antigen; IFN-γ, interferon-γ; MAPK, mitogen-activated protein kinase; PBMC, peripheral blood mononuclear cell; PI3K, phosphatidylinositol 3-kinase; PFS, progression-free survival; STAT, signal transducer and activator of transcription

*Key words:* acquired resistance, CTL epitope, EGFR T790M, immunotherapy, non-small cell lung cancer

## Introduction

Lung cancer is the leading cause of cancer-related deaths worldwide (1). Non-small cell lung cancer (NSCLC) accounts for ~80% of all lung cancer cases. Despite recent development in treatment agents, the prognosis for lung cancer patients remains poor (2).

Overexpression of epidermal growth factor receptor (EGFR) is observed in various malignancies, including lung cancer (3). EGFR activation induces many intracellular signaling pathways, such as the mitogen-activated protein kinase (MAPK), phosphatidylinositol 3-kinase (PI3K), and signal transducer and activator of transcription (STAT) pathways, which cause tumor cell proliferation and survival (4). The EGFR pathway is an appropriate target for cancer therapy, and several agents that block this pathway have been developed. In particular, epidermal growth factor receptor-tyrosine kinase inhibitors (EGFR-TKIs), such as gefitinib and erlotinib, demonstrated marked clinical activity against NSCLC harboring an activating EGFR mutation (5-9). However, patients develop acquired resistance to EGFR-TKIs almost without exception (10). A secondary mutation, resulting in a threonine to methionine change at codon 790 of EGFR (EGFR T790M), is the major mechanism of EGFR-TKI resistance (10,11). Additionally, some reports suggest that the EGFR T790M mutation may not be rare and may exist in a small population of in tumor cells before TKI treatment (12-14). Moreover, a pre-existing T790M mutation was associated with shorter progression-free survival (PFS) in patients receiving TKI treatment (13,14). At this time, no standard treatment for EGFR mutant patients with acquired resistance has yet been established, and novel strategies for overcoming this resistance issue are required.

Immunotherapy for NSCLC patients is considered to be a potentially feasible option, because of its high specificity

and low toxicity against normal tissues; indeed, several tumor-associated antigen (TAA)-targeted phase 2/3 studies are ongoing (15). However, unfortunately, the results of a TAA-based vaccine therapy study were unsatisfactory (16). One concept for improving the effect of cancer vaccine therapy is to target mutated antigen-derived epitopes. It has been reported that various mutated epitopes were recognized by tumor-reactive T cells (17,18), suggesting that the mutated epitope was potentially immunogenic and thus might function as an immunotherapeutic target. There are few studies of immunotherapy targeting the EGFR T790M mutation. Here, we hypothesized that EGFR T790M-harboring cancer cells could be targeted by activated immune cells, and attempted to assess the immunogenicity of the EGFR T790M mutation-derived antigen *in vitro*. In the present study, we identified the human leukocyte antigen (HLA)-A2-restricted EGFR T790M mutation-derived epitope. Our results suggest that immunotherapy targeting the EGFR T790M mutation-derived antigen may be a novel treatment option for NSCLC patients with the T790M mutation. The combination of immunotherapy and EGFR-TKI therapy also may be a novel strategy for prevention of T790M-mediated resistance.

## Materials and methods

*Cell lines*. The human NSCLC cell line H1975 was provided by Professor Seiji Yano (Kanazawa University, Ishikawa, Japan). H1975-A2 (H1975 transfected with HLA-A2) was provided by Dr Tetsuro Sasada (Kurume University, Fukuoka, Japan). Artificial APC-A2 (aAPC-A2) cells, which were generated by transduction of HLA-A*02:01, CD80, and CD83 molecules into K562 cells, were provided by Dr Naoto Hirano (Dana-Farber Cancer Institute, Boston, MA, USA). T2 cells (HLA-A*02:01, TAP$^-$) and human NSCLC cell line 11-18 were purchased from Riken (Saitama, Japan). These cell lines were cultured in RPMI-1640 (Sigma Chemical Co., St. Louis, MO, USA), supplemented with 10% FBS (Gibco-BRL, Carlsbad, CA, USA), 100 U/ml penicillin, and 100 $\mu$g/ml streptomycin in a humidified atmosphere containing 5% $CO_2$.

*PBMC collection*. Peripheral blood samples were collected from four HLA-A*02:01-positive healthy donors, after informed consent was obtained. Peripheral blood mononuclear cells (PBMCs) were isolated by density centrifugation using Ficoll-Hypaque (Pharmacia, Uppsala, Sweden) and frozen in liquid nitrogen until use.

*Epitope prediction and synthesis*. The epitope prediction software BIMAS (http://www-bimas.cit.nih.gov/molbio/hla_bind/) was used to predict peptides that could bind to HLA-A2. EGFR T790M mutation-derived peptides (purity >95%) were purchased from Scrum, Inc. (Tokyo, Japan). H-2 Kb-restricted ovalbumin (OVA) (257-264) (SIINFEKL) peptide (AnaSpec, Inc., Fremont, CA, USA) was used as a negative control in the peptide-binding assay. HLA-A2-restricted cytomegalovirus (CMV) (495-503) (NLVPMVATV) peptide was used as a positive control peptide, and an HLA-A2-restricted HIV-gag (77-85) (SLYNTYATL) peptide (American Peptide Company, Sunnyvale, CA, USA) as an irrelevant peptide in cytotoxic T lymphocyte (CTL) assays.

*Peptide-binding assay*. After incubation in culture medium at 26˚C overnight, T2 cells were washed with PBS and suspended in 1 ml Opti-MEM (Invitrogen Life Technologies, Carlsbad, CA, USA) with peptide (100 $\mu$g/ml), followed by incubation at 26˚C for 3 h and then at 37˚C for 2.5 h. After washing with PBS, HLA-A2 expression was measured using a BD FACSCanto II flow cytometer (BD Biosciences, San Jose, CA, USA) using a FITC-conjugated HLA-A2 (MBL Co., Ltd., Aichi, Japan)-specific monoclonal antibody. Mean fluorescence intensity (MFI) was analyzed using the FlowJo software (Tomy Digital Biology Co., Ltd., Tokyo, Japan). An OVA peptide was used as a negative control. A CMV peptide was used as a positive control peptide.

*Generation of DCs*. CD14$^+$ cells were isolated from PBMCs using human CD14 microbeads (Miltenyi Biotec GmbH, Bergisch Gladbach, Germany). Immature dendritic cells (DCs) were generated from CD14$^+$ cells using IL-4 (10 ng/ml; PeproTech, Inc., Rocky Hill, NJ, USA) and granulocyte-macrophage colony-stimulating factor (GM-CSF) (10 ng/ml; PeproTech, Inc.) in RPMI-1640 supplemented with 10% FBS. Maturation of DCs was induced by prostaglandin E2 (PGE2) (1 $\mu$g/ml; Sigma Chemical Co.) and tumor necrosis factor-$\alpha$ (TNF-$\alpha$) (10 ng/ml; PeproTech, Inc.).

*Induction of peptide-specific CTLs*. CD8$^+$ cells were isolated using human CD8 microbeads (Miltenyi Biotec GmbH) from PBMCs. CD8$^+$ cells ($2x10^6$ cells/well) were stimulated with peptide-pulsed (10 $\mu$g/ml) 100-Gy-irradiated autologous mature DCs ($1x10^5$ cells/well) in RPMI-1640 containing 10% heat-inactivated human AB serum. After 1 week, these cells were stimulated twice weekly with peptide-pulsed (10 $\mu$g/ml) 200-Gy-irradiated aAPC-A2 cells ($1x10^5$ cells/well). Supplementation with 10 IU/ml IL-2 (Proleukin; Novartis, Basel, Switzerland) and 10 ng/ml IL-15 (PeproTech, Inc.) was performed at 3-4-day intervals between stimulations.

*IFN-$\gamma$ ELISPOT assay*. Specific secretion of interferon-$\gamma$ (IFN-$\gamma$) from human CTLs in response to stimulator cells was assayed using the IFN-$\gamma$ enzyme-linked immuno spot (ELISPOT) kit (BD Biosciences), according to the manufacturer's instructions. Stimulator cells were pulsed with peptide for 2 h at room temperature and then washed three times. Responder cells were incubated with stimulator cells for 20 h. The resulting spots were counted using an ELIPHOTO counter (Minerva Tech, Tokyo, Japan).

*CD107a assay and generation of a CTL line*. CD8$^+$ cells isolated using human CD8 microbeads from cultured cells were incubated with peptide-pulsed T2 cells at a ratio of 2:1 for 3.5 h at 37˚C. CD107a-specific antibodies (BD Biosciences) were included in the mixture during the incubation period. CD8$^+$ CD107a$^+$ cells were sorted using a FACSAria II cell sorter (BD Biosciences). Sorted CTLs were stimulated, and the CTL line was established as described previously (19).

*Cytotoxicity assay*. Cytotoxic capacity was analyzed using the Terascan VPC system (Minerva Tech). The CTL line

Table I. Predicted EGFR T790M-derived peptides binding to HLA-A2.

| Peptide name | Position | Length | Sequence | BIMAS score[a] |
|---|---|---|---|---|
| T790M-A | 789-797 | 9 | IMQLMPFGC | 35.378 |
| T790M-B | 790-799 | 10 | MQLMPFGCLL | 51.77 |
| T790M-C | 788-797 | 10 | LIMQLMPFGC | 24.921 |
| T790M-D | 789-797[b] | 9 | IMQLMPFGV | 495.288 |
| T790M-E | 789-797[c] | 9 | IMQLMPFGL | 152.124 |
| T790M-Awt | 789-797 | 9 | ITQLMPFGC | 0.68 |

[a]Binding scores were estimated using the BIMAS software (http://www-bimas.cit.nih.gov/molbio/hla_bind/). [b,c]The cysteine (C) residue at position 797 was mutated to valine (V) and leucine (L), respectively. EGFR T790M, threonine to methionine change at codon 790 of EGFR.

was used as the effector cell type. Target cells were labeled in calcein-AM (Dojindo Molecular Technologies, Inc., Kumamoto, Japan) solution for 30 min at 37°C. The labeled cells were then co-cultured with the effector cells for 4-6 h. Fluorescence intensity was measured before and after the culture period, and specific cytotoxic activity was calculated using the following formula: % cytotoxicity = {1 - [(average fluorescence of the sample wells - average fluorescence of the maximal release control wells)/(average fluorescence of the minimal release control wells - average fluorescence of the maximal release control wells)]} x 100%.

## Results

*Assessment of EGFR T790M-derived peptide binding to HLA-A*02:01 molecules.* As the candidates of HLA-A*02:01-restricted EGFR T790M-derived CTL epitopes, we selected five 9- or 10-mer peptides with high predicted HLA-A*02:01-binding scores, calculated using BIMAS software. Three of the five EGFR T790M-derived peptides had higher binding scores than the corresponding wild-type peptides. Some studies have reported that modified peptides with single amino acid substitutions exhibit improved affinity for HLA molecules and enhanced immunogenicity (20-22); thus, we also designed two modified peptides. These modified peptides with a substitution of Cys for Val (T790M-D) or Leu (T790M-E) at codon 797 showed higher binding scores (Table I).

Using the HLA-A2 TAP-deficient T2 cell line, the binding affinity of the five synthetic peptides to HLA-A2 was assessed. A peptide-binding assay showed that three EGFR T790M-derived peptides were able to bind to HLA-A*02:01 molecules. In particular, the binding capability of the T790M-A peptide to HLA-A*02:01 molecules was higher than that of the corresponding wild-type peptide. This result suggests that the single amino acid substitution at codon 790 improved the binding affinity for HLA-A*02:01 molecules. The binding affinities of two mutated peptides (T790M-D and -E) to HLA-A*02:01 were equivalent to that of the CMV peptide used as a positive control (Fig. 1).

*Induction of EGFR T790M-derived peptide-specific CTLs from human PBMCs.* To evaluate the immunogenic potential of the five predicted HLA-A*02:01-binding peptides derived from EGFR T790M, we attempted to induce peptide-specific

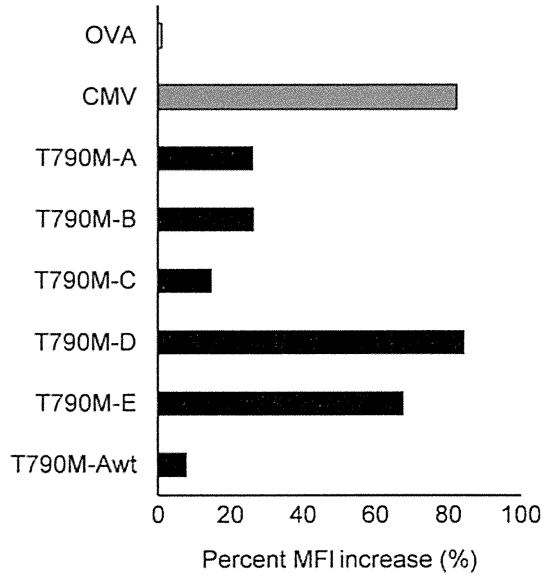


Figure 1. Binding of threonine to methionine change at codon 790 of EGFR (EGFR T790M)-derived peptides to human leukocyte antigen (HLA)-A2 molecule. A T2 binding assay was performed using a FACS system. An ovalbumin (OVA) peptide was used as a negative control. The bars show percent increases in mean fluorescence intensity (MFI). The average of two independent experiments is shown. (Percent MFI increase) = (MFI with the given peptide - MFI without peptide)/(MFI without peptide) x 100.

CTLs from human PBMCs obtained from four healthy donors. Several reports have shown the usefulness of artificial antigen-presenting cells (aAPCs) for the induction and expansion of peptide-specific CTLs from PBMCs (23,24). Thus, we attempted to induce such CTLs using aAPCs. $CD8^+$ cells were isolated from human PBMCs using human CD8 microbeads, and then stimulated with peptide-pulsed DCs for 1 week and subsequently, stimulated twice weekly with peptide-pulsed aAPC-A2 (Fig. 2A). As shown in Fig. 2B, ELISPOT assays revealed that T790M-A (789-797) (IMQLMPFGC)-specific CTLs were induced from PBMCs from all four donors. Also, induction of T790M-B (790-799) (MQLMPFGCLL)-specific CTLs were induced from PBMCs from two of the four healthy donors. However, stimulation with three other peptides, including modified peptides, did not induce peptide-specific CTLs. These results suggest that T790M-A (789-797) and T790M-B (790-799) have immunogenic potential and that

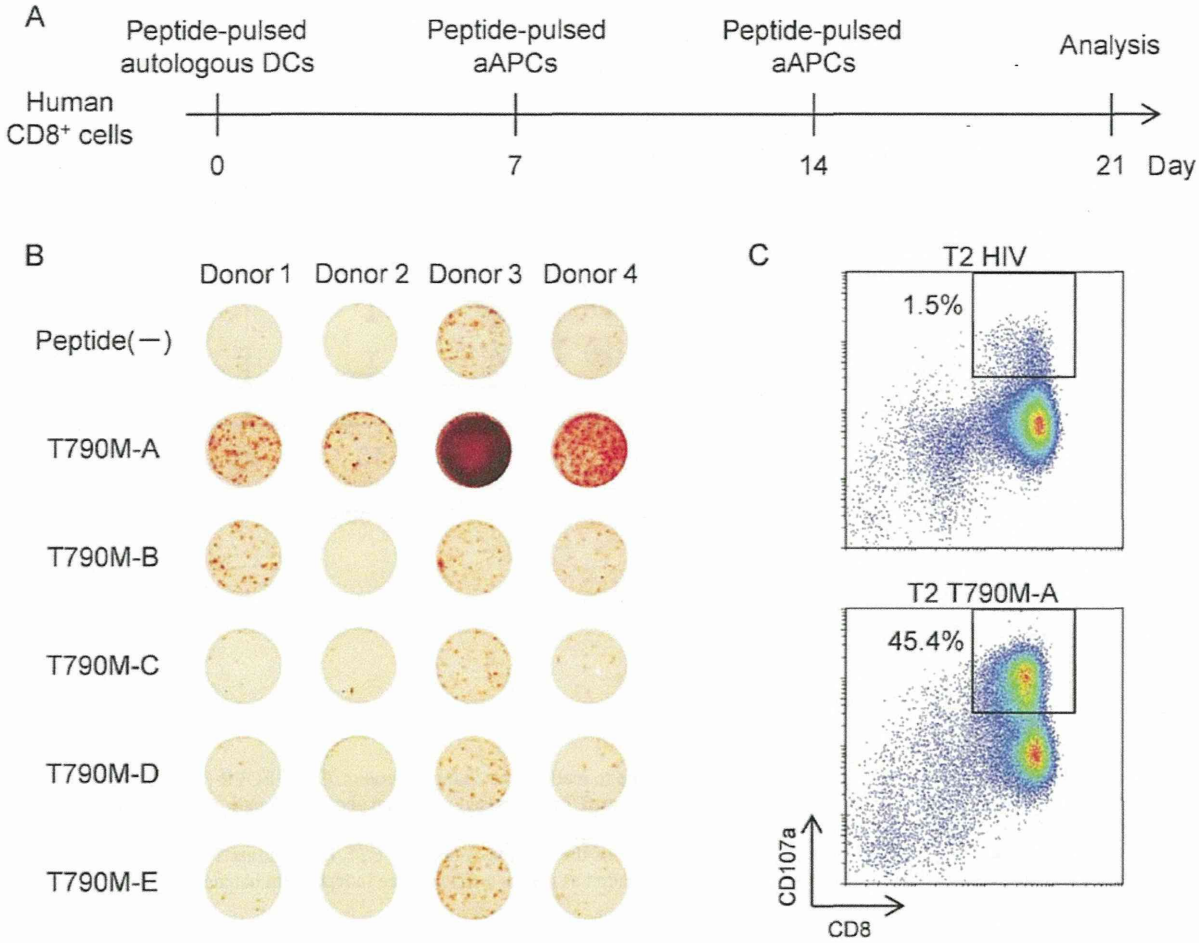


Figure 2. Induction of threonine to methionine change at codon 790 of EGFR (EGFR T790M)-derived peptide-specific cytotoxic T lymphocytes (CTLs) from peripheral blood mononuclear cells (PBMCs) of healthy donors. (A) Induction schedule of peptide-specific CTLs. $CD8^+$ cells ($2x10^6$ cells) isolated by anti-human CD8 microbeads from PBMCs were incubated with 10 $\mu$g/ml peptide-pulsed autologous dendritic cells (DCs) ($1x10^5$ cells) on day 0, followed by incubation with 10 $\mu$g/ml peptide-pulsed artificial antigen-presenting cell (aAPCs) ($1x10^5$ cells) on days 7 and 14. Peptide specificity was assessed by interferon-γ (IFN-γ) enzyme-linked immuno spot (ELISPOT) assay on day 21. (B) IFN-γ ELISPOT assay was carried out (effector, $1x10^5$ cells/well; target, $1x10^5$ cells/well) in duplicate at least three times independently; representative data are shown. (C) T790M-A-specific CTLs of healthy donor 3 were incubated with 10 $\mu$g/ml peptide-pulsed T2 cells (E:T = 2:1) for 3.5 h in the presence of an anti-human CD107a antibody. $CD8^+$ $CD107a^+$ cells were sorted using a FACSAria II cell sorter, which resulted in establishment of a T790M-A-specific CTL line.

CTLs specific for these peptides can be induced from human PBMCs. Given the effective induction of T790M-A (789-797) peptide-specific CTLs, we performed further analysis of the T790M-A peptide.

*Generation of EGFR T790M-A-specific CTL line from human PBMCs*. Next, we attempted to generate a purified T790M-A (789-797)-specific CTL line. Because the surface mobilization of CD107a is useful for identifying and isolating functional tumor-reactive T cells (25), we performed a CD107a assay to generate a purified T790M-A (789-797)-specific CTL line. Cultured cells stimulated by T790M-A peptide-pulsed DCs and aAPC-A2 *in vitro* were incubated with peptide-pulsed T2 cells at a ratio of 2:1 for 3.5 h at 37˚C in the presence of an anti-CD107a antibody. More frequent $CD107a^+$ cells were observed when CTLs were co-cultured with T790M-A peptide-pulsed T2 cells compared to HIV-peptide-pulsed T2 cells, and $CD8^+$ $CD107a^+$ cells were sorted as a purified, peptide-specific CTL line using a FACSAria II cell sorter (Fig. 2C). A purified T790M-A-specific CTL line was established from healthy donor 3.

*Cross-reactivity of the T790M-A-specific CTL line with other EGFR T790M-derived peptides*. To assess its cross-reactivity with other EGFR T790M-derived peptides, the T790M-A-specific CTL line was cultured with T2 cells pulsed with each peptide, and IFN-γ production was measured by ELISPOT assay. The T790M-A-specific CTL line specifically recognized T2 cells pulsed with T790M-A (789-797) but not non-peptide-pulsed T2 cells. The T790M-A-specific CTL line did not recognize T2 cells pulsed with the T790M-A (789-797) wild-type (ITQLMPFGC) peptide. Also, T2 cells pulsed with T790M-B, -D, and -E were not recognized by the T790M-A-specific CTL line (Fig. 3A). However, the T790M-A-specific CTL line showed cross-reactivity with T2 cells pulsed with T790M-C.

Next, we evaluated the cytolytic activity of the T790M-A-specific CTL line against cognate peptide-pulsed T2 cells. The T790M-A-specific CTL line specifically lysed T790M-A peptide-pulsed T2 cells but not HIV-peptide-pulsed T2 cells (Fig. 3B). These results suggest that the T790M-A-specific CTL line showed cross-reactivity against some EGFR

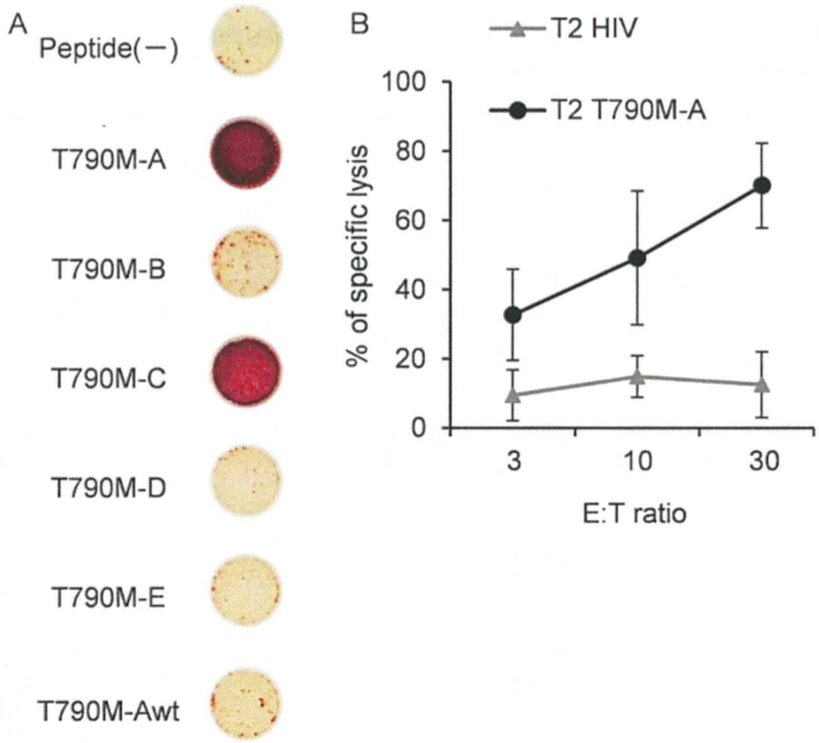


Figure 3. Cross-reactivity of the T790M-A-specific CTL line with threonine to methionine change at codon 790 of EGFR (EGFR T790M)-derived peptides. (A) Interferon-γ (IFN-γ) enzyme-linked immuno spot (ELISPOT) assay against T2 cells pulsed with each peptide. T2 cells pulsed with EGFR T790M-derived peptides (EGFR T790M-A, -B, -C, -D, -E, and Awt) were used as the target (effector $1x10^4$ cells/well, target $1x10^4$ cells/well). The assays were carried out in duplicate wells, and representative data are shown. (B) Cytotoxicity of the T790M-A-specific CTL line against T790M-A peptide-pulsed T2 cells. HIV-peptide-pulsed T2 cells were used as a negative control. Data are presented as means ± SD of three independent batches.

T790M-derived peptides, but not the corresponding wild-type EGFR-derived peptide. This cross-reactivity seems to be favorable for efficacy against EGFR T790M$^+$ cancer cells.

*The T790M-A-specific CTL line recognizes and lyses HLA-A2$^+$ T790M$^+$ NCSLC cells.* Next, we assessed the ability of the T790M-A-specific CTL line to recognize the HLA-A2$^+$ T790M$^+$ NCSLC cell line. This CTL line was incubated with 11-18 (T790M$^-$, HLA-A2$^+$), T790M-A-pulsed 11-18, H-1975 (T790M$^+$ HLA-A2$^-$), or H-1975-A2 (T790M$^+$ HLA-A2$^+$), and IFN-γ production was evaluated. We confirmed that the T790M-A-specific CTL line recognized peptide-pulsed 11-18 and H-1975-A2, but not 11-18 and H-1975, cells by IFN-γ ELISPOT assay (Fig. 4A). Similar data were obtained using CTLs from healthy donor 1 stimulated with T790M-A peptide-pulsed DC and aAPC-A2 *in vitro*, which were not purified by the CD107a assay (data not shown).

To evaluate the function of the T790M-A-specific CTL line against H1975-A2, a CD107a assay was performed. CD107a$^+$ cells were detected more frequently in culture with H-1975-A2 than with H-1975 cells (Fig. 4B).

Finally, we investigated the cytotoxic activity of the T790M-A-specific CTL line against H-1975-A2. Target cells were labeled with calcein-AM and co-cultured with the effector cells for 4-6 h. The T790M-A-specific CTL line showed cytotoxic activity against H1975-A2 cells, but not H1975 cells (Fig. 4C). These results suggest that the T790M-A-specific CTL line can recognize NSCLC cells harboring the EGFR T790M mutation in an HLA-A2-restricted manner.

## Discussion

Mutated antigens associated with tumor cell progression and survival or drug resistance represent novel targets for cancer vaccine therapy. Warren *et al* evaluated computationally the antigenic potential of somatic mutations that occur in human cancers (26). They showed that several gene mutation-derived epitopes have immunogenic potential, at least computationally. Moreover, point mutations within the ABL kinase domain of the *BCR-ABL* gene are the most common causes of resistance to imatinib in chronic myeloid leukemia (CML) patients (27). Cai *et al* reported that the mutated *BCR-ABL* gene was associated with a TKI-resistance-generated CTL epitope in CML patients (28). These results suggest new immunotherapeutic approaches based on a TKI-resistant mutation-derived neoantigen. That is, mutations associated with acquired resistance to TKI therapy can be targeted by immune-based treatment strategies. This strategy may be an option to treat the gene mutation-mediated drug-resistant cancer cells. In the present study, we demonstrated the immunogenicity of antigens from mutated EGFR that are involved in TKI resistance in NCSLC.

TAAs can be classified into several categories, such as cancer-testis (CT) antigens, overexpressed antigens, differentiation antigens, and mutated antigens. Of these, only mutated antigens are unique, because they are not expressed in normal tissues. Previous reports have shown that peptide vaccine therapy can occasionally induce ineffective CTL responses, contrary to expectations (29-31). One possibility is

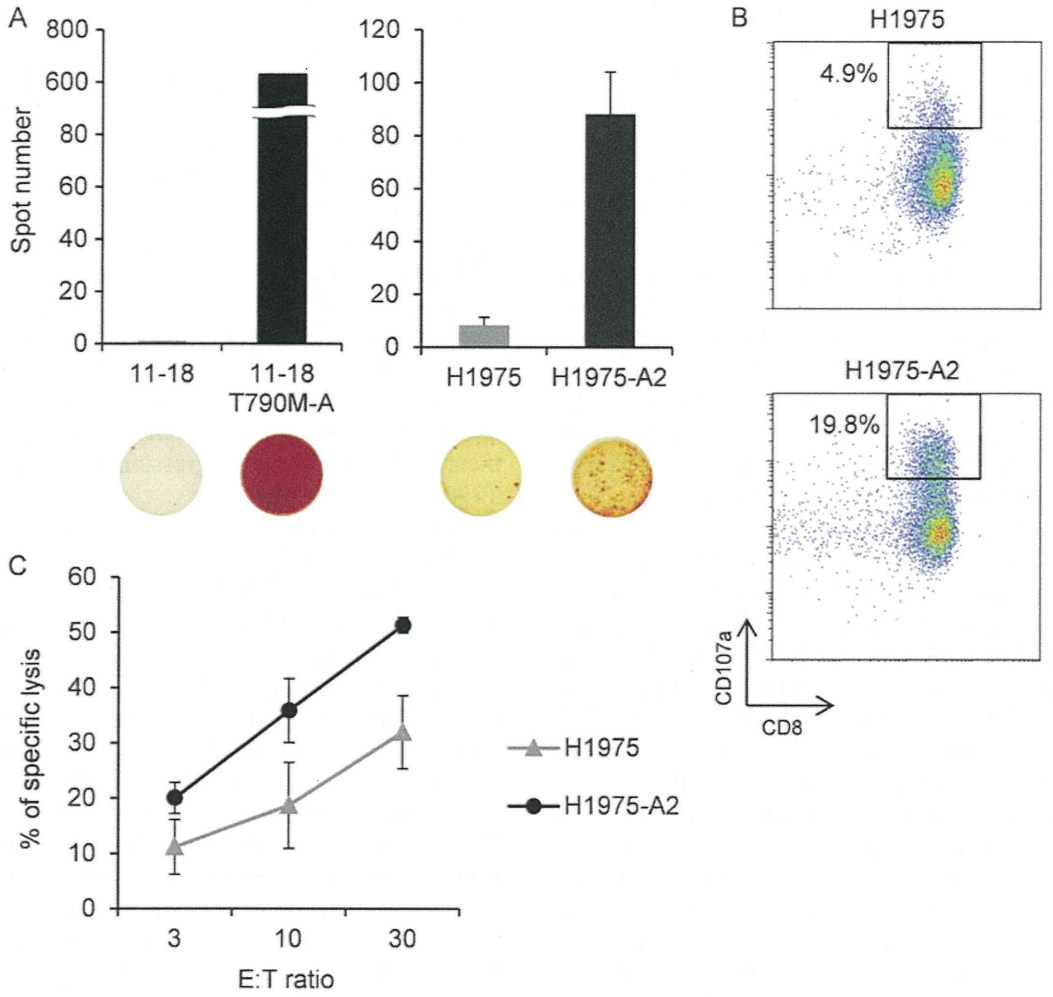


Figure 4. Reactivity of the T790M-A-specific CTL line against non-small-cell lung cancer (NSCLC) cells with or without the T790M mutation. (A) Interferon-γ (IFN-γ) enzyme-linked immuno spot (ELISPOT) assay results for the $T790M^+$ and $T790M^-$ NSCLC lines. Left: 11-18 and T790M-A peptide-pulsed (10 μg/ml) 11-18 cells were used as the targets (effector $1x10^5$ cells/well, target $1x10^5$ cells/well). Right: H-1975 and H1975-A2 cells were used as the targets (effector, $5x10^4$ cells/well; target, $5x10^4$ cells/well). The bars indicate the IFN-γ ELISPOT counts. (B) CD107a assay of the $T790M^+$ NSCLC line (E:T = 2:1). $CD8^+$ $CD107a^+$ cells were gated. (C) Cytotoxicity against the $T790M^+$ NSCLC cell line at the indicated effector/target ratios. Data are presented as means ± SD of three independent batches.

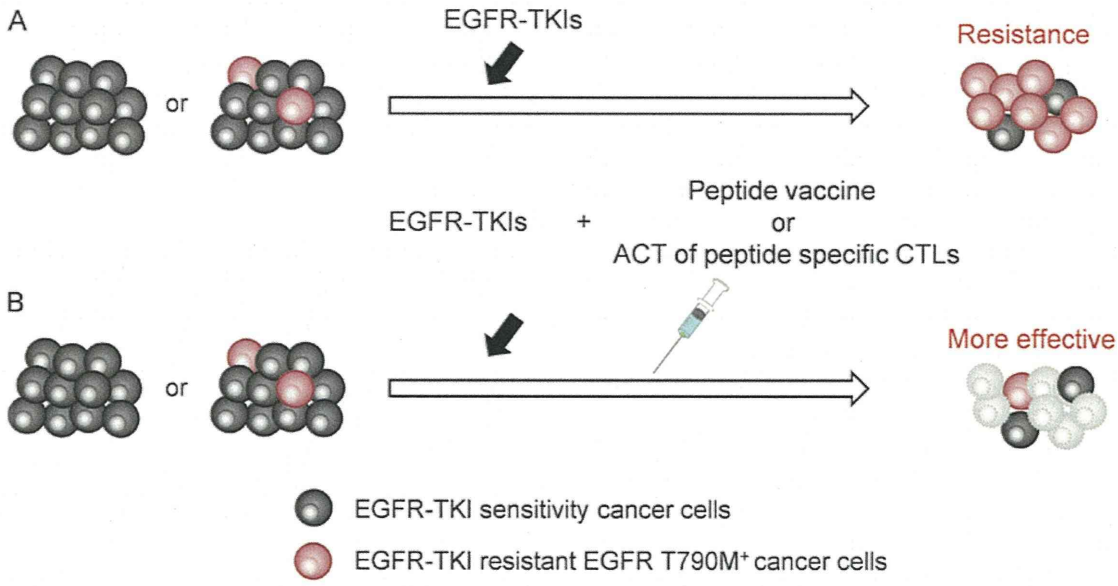


Figure 5. Combination therapy of epidermal growth factor receptor-tyrosine kinase inhibitor (EGFR-TKI) with T790M-targeted immunotherapy. (A) Generally, cancer cells develop acquired resistance to EGFR-TKI. (B) TKI-resistant cells harboring the T790M mutation were targeted by immunotherapy. This combination therapy may be effective against cancers with and without the threonine to methionine change at codon 790 of EGFR (EGFR T790M) mutation.

that the induced antigen-specific CTLs have a low affinity, and thus recognize only target cells pulsed with high concentrations of the peptide and not naturally presented epitopes on tumor cells. Several EGFR-derived CTL epitopes have been identified (32,33); however, the frequency of high-avidity EGFR-specific CTLs seems to be low in patients with EGFR-expressing cancers, because EGFR is a self-antigen that induces tolerance. The ability of low-avidity CTLs to recognize antigen-expressing tumor cells is considered to be weak. However, mutation-derived antigens are not self-antigens; thus, they would not be expected to induce immunotolerance, and so may have high immunogenicity. Indeed, in melanoma patients who experienced dramatic therapeutic effects after adoptive cell therapy with tumor-infiltrating lymphocytes (TILs), the mutated antigen-derived epitope was immunodominant and was recognized by tumor-reactive T cells (34,35).

In the present study, BIMAS was used to select EGFR T790M-derived candidate peptides that bind to HLA-A*02:01 according to computer algorithms, and T790M-A-specific CTLs could be induced from PBMCs of all four healthy donors by stimulation with peptide-pulsed DCs and aAPCs. Amino acid substitution of anchor residues (at position 2 and the C-terminus for HLA-A2) can alter the binding affinity (36-38). Leucine and methionine are the preferred anchor residues at position 2 of HLA-A2 (36,37). T790M-A (IMQLMPFGC) harbors a substitution of threonine to methionine at the anchor site, which confers immunogenicity. Also, valine and leucine are the preferred anchor residues at the C-terminus (36,37).

Then, we designed the modified peptides, T790M-D (IMQLMPFGV, substitution of cysteine to valine at the C-terminus) and T790M-E (IMQLMPFGL, substitution of cysteine to leucine at the C-terminus). These peptides bound to the HLA-A*02:01 molecule strongly (Fig. 1), but could not induce specific CTLs. T790M-D and -E are not self-antigens, being similar in this respect to T790M-A; this difference may be due in part to the difference in the frequency of peptide-specific CTL precursors. To confirm that the predicted candidate peptides are naturally presented peptides on tumor cells, peptide-specific CTL clones or lines induced by the peptides must recognize the tumor cells. A mass spectrometry (MS)-based method facilitates identification of peptide presentation by tumor cells (39). In this study, we confirmed the peptide-specific recognition of tumor cells by a peptide-specific CTL line, but not a CTL clone. However, CTL lines may contain distinct CTL clones that recognize irrelevant peptides, leading to apparent tumor reactivity (40). To avoid misleading tumor recognition and to evaluate the antigen-specific response of a CTL line, we used a peptide-specific CTL line established by CD107a sorting. An IFN-γ ELISPOT assay suggested that the specific CTL line recognized NSCLC cells harboring the EGFR T790M mutation in an HLA-A*02:01-restricted manner.

The T790M-A-specific CTL line did not show activity against the corresponding wild-type peptide. This suggests that EGFR T790M-targeted immunotherapy has no effect on NSCLC prior to EGFR-TKI treatment, with the exception of any pre-existing population of T790M-harboring cells, at least theoretically. Thus, consideration of combination therapy, EGFR-TKI and EGFR T790M-targeted immunotherapy, seems reasonable. Several studies have suggested that combination therapy could improve the efficacy of cancer immunotherapy. For instance, some chemotherapeutic agents can lead to upregulation of TAA expression or improvement of tumor cell resistance to specific CTLs (41). Use of an EGFR-TKI or anti-EGFR antibody augments the IFN-γ-induced expression of MHC classes I and II by A431 malignant human keratinocytes (42). Moreover, gefitinib improved the cytotoxic activity of natural killer cells against H1975 by modulating the interaction between NK cells and cancer cells, and by inhibiting STAT3 expression (43). These results indicate that the combination of EGFR-TKI and immunotherapy may have synergistic activity against NSCLC cells. The concept of combination therapy is shown in Fig. 5. Adding EGFR T790M-targeted immunotherapy to EGFR-TKI treatment could control the progression of cancer cells harboring T790M.

Yamada *et al* reported two HLA-A2-restricted EGFR T790M-derived CTL epitopes (790-799 MQLMPFGCLL and 788-798 LIMQLMPFGCL) (44). In addition to these epitopes, we identified the HLA-A*02:01-restricted CTL epitope T790M-A (789-797 IMQLMPFGC). We found that a T790M-A-specific CTL line established from human PBMCs had the ability to recognize and lyse the HLA-A*02:01$^+$ T790M$^+$ NCSLC cell line, and importantly, did not show cross-reactivity with the corresponding wild-type EGFR peptide. These results suggest that the EGFR T790M-A-specific CTL line recognizes single amino acid substitutions, leading to a low level of auto-immune reaction. The combination of an EGFR-TKI and T790M-targeted immunotherapy may be useful for treatment of NSCLC with the T790M mutation.

## Acknowledgements

We thank Professor Seiji Yano for providing the NSCLC cell line H1975, Dr Tetsuro Sasada for providing the NSCLC cell line H1975-A2, and Professor Naoto Hirano for providing aAPC-A2. This study was supported in part by the National Cancer Center Research and Development Fund (25-A-7), as well as Research for the Promotion of Cancer Control Programmes, Research on Applying Health Technology, and Third Term Comprehensive Control Research for Cancer from the Ministry of Health, Labour, and Welfare, Tokyo, Japan.

## References

1. Jemal A, Siegel R, Ward E, Murray T, Xu J and Thun MJ: Cancer statistics, 2007. CA Cancer J Clin 57: 43-66, 2007.
2. Youlden DR, Cramb SM and Baade PD: The international epidemiology of lung cancer: geographical distribution and secular trends. J Thorac Oncol 3: 819-831, 2008.
3. Normanno N, Maiello MR and De Luca A: Epidermal growth factor receptor tyrosine kinase inhibitors (EGFR-TKIs): simple drugs with a complex mechanism of action? J Cell Physiol 194: 13-19, 2003.
4. Hynes NE and Lane HA: ERBB receptors and cancer: the complexity of targeted inhibitors. Nat Rev Cancer 5: 341-354, 2005.
5. Mok TS, Wu YL, Thongprasert S, *et al*: Gefitinib or carboplatin-paclitaxel in pulmonary adenocarcinoma. N Engl J Med 361: 947-957, 2009.
6. Mitsudomi T, Morita S, Yatabe Y, *et al*: Gefitinib versus cisplatin plus docetaxel in patients with non-small-cell lung cancer harbouring mutations of the epidermal growth factor receptor (WJTOG3405): an open label, randomised phase 3 trial. Lancet Oncol 11: 121-128, 2010.